

Tertiary Mafic Lavas of Turkana, Kenya: Constraints on East African Plume Structure and the Occurrence of High- μ Volcanism in Africa

TANYA FURMAN^{1,*}, KELLY M. KALETA², JULIA G. BRYCE³ AND BARRY B. HANAN⁴

¹DEPARTMENT OF GEOSCIENCES, PENNSYLVANIA STATE UNIVERSITY, UNIVERSITY PARK, PA 16802, USA

²SHELL EXPLORATION AND PRODUCTION COMPANY, 200 N. DAIRY ASHFORD, HOUSTON, TX 77079, USA

³DEPARTMENT OF EARTH SCIENCES, UNIVERSITY OF NEW HAMPSHIRE, DURHAM, NH 03824, USA

⁴DEPARTMENT OF GEOLOGICAL SCIENCES, SAN DIEGO STATE UNIVERSITY, SAN DIEGO, CA 92182, USA

RECEIVED SEPTEMBER 16, 2004; ACCEPTED FEBRUARY 13, 2006
ADVANCE ACCESS PUBLICATION MARCH 21, 2006

The East African Rift System is important to understanding plume-initiated rifting as manifest in the geochemistry of mafic lavas erupted along the rift throughout its evolution. We present new data from high-MgO Tertiary lavas from Turkana, northern Kenya, to investigate regional melt source components, to identify the depths and degrees of melting, and to characterize spatially and temporally the chemical structure of the underlying mantle. The Turkana area is a region of high lithospheric extension that sits between two topographic uplifts thought to be surface expressions of one or more upwelling mantle plumes. Thinning of local crust is believed to be accompanied by widespread removal of the mantle lithosphere, causing the asthenosphere to be in close contact with the overlying crust. New geochemical data on basanites, picrites and basalts (MgO > 7 wt %) tightly constrain the primary melt source regions of Tertiary volcanism. Initial isotopic signatures ($^{143}\text{Nd}/^{144}\text{Nd} = 0.51267\text{--}0.51283$, $^{87}\text{Sr}/^{86}\text{Sr} = 0.7031\text{--}0.7036$) and trace element abundances (Ce/Pb ~ 30 , La/Nb = 0.6–0.8 and Ba/Nb = 3–10) in these lavas are consistent with derivation from sub-lithospheric sources. Basalts and picrites erupted between ~ 23 and 20 Ma have Sr–Nd–Pb–He isotopic characteristics indicative of high- μ influence, record high depths and degrees of partial melting, and are associated with rift propagation to the north and south. Accordingly, these lavas sample a source region that is geochemically distinct from that reflected both in Oligocene Ethiopian flood basalts and in the modern Afar region. The geochemical data support numerical and theoretical models as well as

tomographic results providing for a complex thermal structure in the mantle beneath East Africa and are interpreted to reflect isotopically distinct plume heads beneath Tanzania and Afar that are derived from the chemically heterogeneous South African superplume.

KEY WORDS: East African Rift System; mantle plumes; HIMU; geochemistry; Afar

INTRODUCTION

The East African Rift system is a classic recent example of continental rifting, and provides an excellent framework in which to investigate extensional magmatism. Voluminous and/or thick successions of basalts crop out from northern Ethiopia to southern Tanzania, and span pre-rift, syn-rift and post-rift periods. The Turkana Depression in northern Kenya is a region of anomalously high extension, forming a broad (~ 150 km wide), diffuse fault zone that is nearly three times the width of the rift observed in other areas. This highly extended region sits between two topographic uplifts (Fig. 1), thought to be surface expressions of an underlying mantle plume (e.g. Thiessen *et al.*, 1979). The Turkana Depression is part of a failed Mesozoic rift system, allowing for the possibility

*Corresponding author. Telephone: 814-865-5782. Fax: 814-863-7823. E-mail: furman@geosc.psu.edu

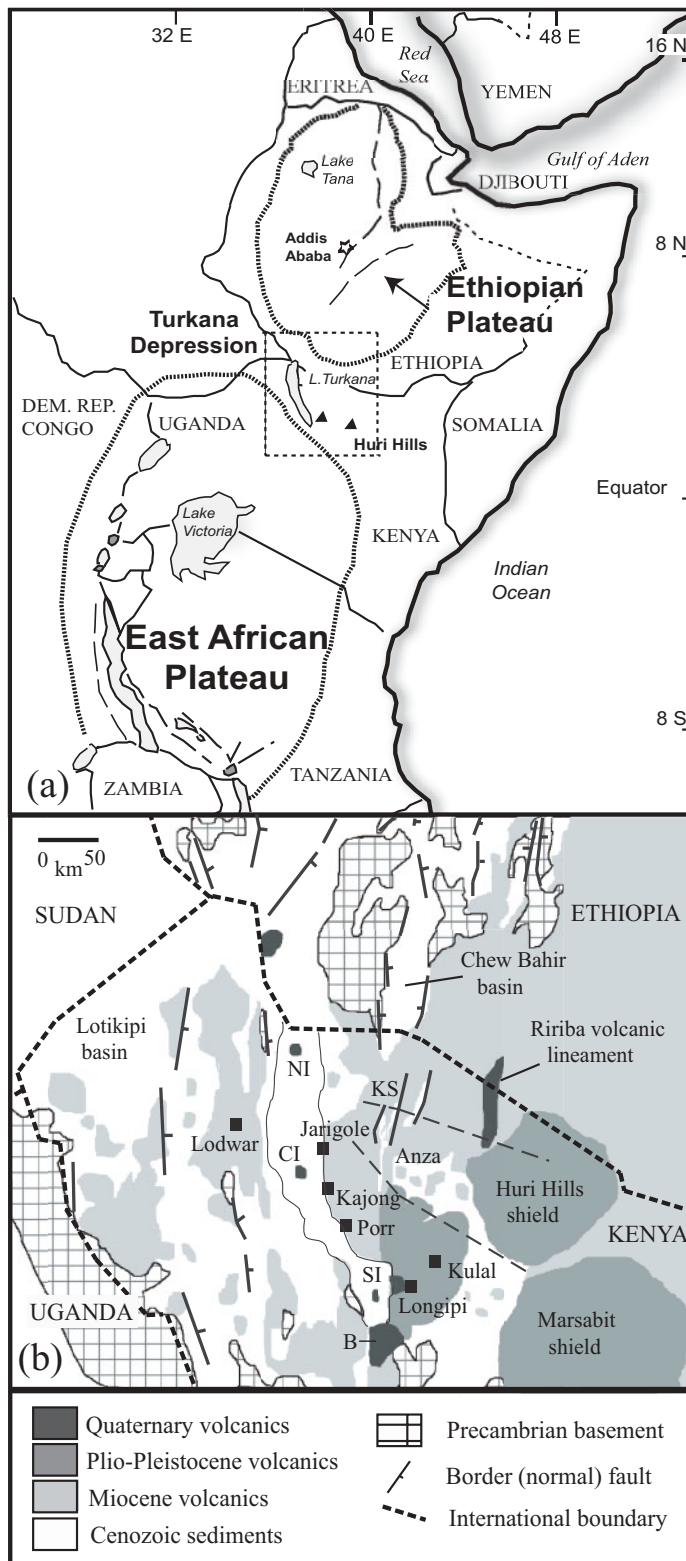


Fig. 1. (a) Sketch map of the East African Rift System. Bold dotted lines enclose areas of the Ethiopian and Kenyan plateaux with elevation >1 km (after Ebinger *et al.*, 2000). Major structural features of the Rift are indicated with dashed lines. (b) Geological features of the Turkana rift. ■, Eocene to Pliocene sample localities; Quaternary volcanic centers within Lake Turkana are labeled (NI, North Island; CI, Central Island; SI, South Island; B, the Barrier). KS, Kino-Sogu fault zone.

that the plateaux are actually part of one large zone of uplift extending from southern Africa to the Red Sea (e.g. Nyblade & Robinson, 1994; Gurnis *et al.*, 2000). By documenting spatial and temporal variations in the magmatic source regions contributing to Turkana mafic volcanism we gain important insight into the temporal evolution of plume-driven rifting in East Africa.

Volcanism in the Turkana Depression occurred in three distinct episodes. The first took place in the Early Oligocene (between ~40 and 30 Ma) prior to initiation of widespread rifting in the Late Oligocene to Early Miocene (~25–20 Ma; Morley *et al.*, 1992), and is manifest locally in northern Kenya and southern Ethiopia (Morley *et al.*, 1992; George *et al.*, 1998). A second, more voluminous, phase took place between roughly 26 and 16 Ma. This magmatic and tectonic episode apparently propagated northward from Kenya into southern Ethiopia, where it is reflected in a volcanic pulse between 20 and 11 Ma (Stewart & Rogers, 1996; George *et al.*, 1998), as well as southward into the Kenya and Western Rifts. The third phase of volcanism began in the Plio-Pleistocene (~3.5 Ma) and continues at present; recent magmatism occurs in several discrete areas (Fig. 1). These three magmatic events are spatially overlapping, but are characterized by lavas with distinct geochemical features.

Our primary objective is to place constraints on the long-term thermal, mineralogical and chemical evolution of the melt source region(s) beneath this highly extended portion of the African Rift. Despite the tectonic significance of the Turkana Depression, and the extensive history of both rifting and volcanism, geochemical studies of mafic lavas from this area are limited (Bloomer *et al.*, 1989; Karson & Curtis, 1994; Furman *et al.*, 2004). We employ new major and trace element data as well as Sr–Nd–Pb–He isotopic ratios to explore the nature of the mantle source region, document its heterogeneities, and infer its temporal evolution. In particular, we investigate the HIMU-like isotopic signature of Miocene picrites ($^{206}\text{Pb}/^{204}\text{Pb} \sim 20.4$, $^{208}\text{Pb}/^{204}\text{Pb} \sim 40$ and $^{87}\text{Sr}/^{86}\text{Sr} \sim 0.7032$) and determine the origin of widespread African volcanism with this isotopic character (e.g. Janney *et al.*, 2002). Morley (1994) interpreted structural aspects of early Turkana volcanism to suggest a link to the mantle plume that impacted beneath northern Ethiopia at ~30 Ma. This interpretation is consistent with numerical modeling (Ebinger & Sleep, 1998) that suggests that Cenozoic to Recent magmatism in eastern and west-central Africa is associated with a single large mantle plume. In contrast, George & Rogers (2002) interpreted the geochemistry of the oldest (45 to 30 Ma) southern Ethiopian mafic lavas to require two distinct mantle plumes, one at present beneath Afar and a second plume below the Turkana Depression. Recent tomographic studies also suggest that there are two distinct thermal

anomalies that extend to mid-mantle depths—one beneath the Afar and the other located beneath central Kenya (Debayle *et al.*, 2001; Nyblade *et al.*, 2000; Montelli *et al.*, 2004). The results from Turkana provide critical insight into this debate because of the long history of volcanism in this area and its unique geographical position in the inter-domal region of the East African Rift.

TECTONIC SETTING

The Turkana Rift lies at the northern terminus of the eastern arm of the East African Rift system (Fig. 1). This site is tectonically unusual within this region in that it has had a prolonged rifting history. Earliest documented rifting began to the east of the modern rift axis when the Anza graben developed during the Cretaceous. Reactivation of existing Anza faults and formation of new grabens have both occurred in Neogene time. Miocene–Recent fault systems initiated in the Lotikipi basin around 25 Ma have generally propagated south-eastward through time to the Kinu Sogo fracture zone, the southern terminus of the main Ethiopian Rift (Fig. 1). Seismic surveys carried out by Project PROBE, however, found a significant rift structure underlying Lake Turkana (Dunklema *et al.*, 1988) that suggests the area is a northern continuation of the Kenya Rift (Morley *et al.*, 1992; Hendrie *et al.*, 1994). This modern rift is characterized by a series of half-grabens that alternate polarity along the length of Lake Turkana. Individual rift basins are approximately 20 km long and 10 km wide, and Quaternary volcanism occurs at basin midpoints, forming discrete volcanic centers that are axially aligned with a spacing of 51 ± 6 km (Dunklema *et al.*, 1988).

The modern Turkana rift is about 150 km wide. The superposition of three distinct rifting episodes in North Kenya (Late Jurassic–Cretaceous, Paleogene and Miocene–Recent) has produced cumulative stretching factors approaching two (Ebinger & Ibrahim, 1994). Maximum stretching factors calculated for episodic extension in Turkana increase from ~1.25 for the Paleogene to ~1.4 at the end of the Miocene, and reach a maximum value of ~1.6 for the late Pliocene (Hendrie *et al.*, 1994). The cumulative stretching factor approaches the theoretical limit for decompression melting during adiabatic upwelling of asthenosphere of 'normal' potential temperature (1280°C; McKenzie & Bickle, 1988), but the episodic values are substantially lower. These observations suggest that a region of elevated mantle temperatures has been needed to generate basalt lavas throughout the history of Turkana magmatism. We demonstrate below that the geochemistry of Tertiary Turkana lavas supports the influence of a mantle plume rather than the presence of anomalous (i.e. hydrated) mantle that is readily melted at normal ambient mantle temperatures.

GEOLOGY AND PETROLOGY OF TERTIARY VOLCANIC CENTERS

Magmatism in Turkana was widespread in the Tertiary, but occurred in a restricted series of eruptive centers during the Quaternary (Fig. 1). Earliest volcanism in western Turkana preceded half-graben rift formation by some 10–15 Myr (Brotzu *et al.*, 1984; Morley *et al.*, 1992). Volcanism in Turkana comprises fissure-derived flood basalts as well as products from discrete composite volcanic centers. A wide range of eruptive products exist in the Tertiary Turkana suite, with abundant rhyolitic lavas and pyroclastics present at most locations.

In this study we focus on ~50 mafic lavas from seven eruptive areas located primarily on the eastern side of Lake Turkana, spanning three discrete volcanic episodes over a time period of almost 40 Myr (Table 1). The oldest lavas investigated (32–40 Ma) are from the Kajong area and Mt. Porr in the south-central portion of the Turkana Rift, and comprise part of the Balsea Kormoto basalts (Table 1; Walsh & Dodson, 1969; Ochieng' *et al.*, 1988). A second volcanic episode is characterized by primitive mafic lavas from Lodwar, west of Lake Turkana (23–26 Ma), and from Jarigole, east of the lake (17–23 Ma; Ochieng' *et al.*, 1988) (Fig. 1). The Jarigole Plateau comprises some 400 m of flood basalts interspersed with alkaline dikes and plugs as well as nepheline syenite intrusives (Ochieng' *et al.*, 1988; Wilkinson, 1988). Lavas from nearby Allia Bay and Loiyangalani are also probably early to mid-Miocene in age (P. Curtis, personal communication, 1996). Finally, at the southern end of Lake Turkana, the early Pliocene Longipi basalts erupted from cinder cones to form the Longipi shield (Table 1; Fig. 1); volcanic sequences here thicken to the north, forming beds in excess of 300 m (Ochieng' *et al.*, 1988). Adjacent to Longipi is the elongate Mt. Kulal shield, where several cones have produced mid-Pliocene to Quaternary basalts, tuffs and pumice lapilli (beginning at ~2.9 Ma; Ochieng' *et al.*, 1988).

The majority of samples used in this study are non-vesicular and nearly aphanitic, with <5 vol. % phenocrysts (0.5–2 mm) of olivine, plagioclase feldspar and, less commonly, clinopyroxene in a fine-grained matrix of olivine, plagioclase feldspar, clinopyroxene and opaque oxides. MgO-rich samples from Jarigole and Lodwar contain up to 20 vol. % euhedral olivine crystals ranging up to 8 mm in length. Accumulated olivine phenocrysts in the two highest-MgO picrites have an average composition of $\text{Fo}_{85.4 \pm 2.3}$ (based on 12 grains analyzed in triplicate); moderately high CaO contents of these olivines (0.30–0.47 wt %) indicate that they are accumulative from melts rather than entrained mantle xenocrysts (Thompson & Gibson, 2000). Kajong lavas comprise two groups: Group A samples (KJ 1, KJ 13 and KJ 16) have devitrified matrix glass that is locally altered with

veins of trace calcite. The remaining Kajong samples are holocrystalline and fresh; alteration is not observed in samples from other areas.

SAMPLING AND ANALYTICAL TECHNIQUES

All samples were collected by P. Curtis and J. Karson as part of a structural investigation of the Turkana area. Samples used in our study were selected from over 350 available specimens on the basis of freshness and spatio-temporal control, and are biased towards mafic lavas with visible modal olivine.

Sample preparation involved crushing centimetre-thick slabs that had been polished to remove saw marks, and then powdering the chips in a WC disc mill. Bulk-rock analyses for major and minor elements were obtained by direct current plasma (DCP) and inductively coupled plasma mass spectrometry (ICP-MS) at Duke University (Table 1; see Appendix for details). Sr–Nd–Pb isotopic analyses (Table 2) were performed at the Keck Center for Geochemistry in the Department of Earth and Space Sciences at the University of California, Los Angeles using conventional thermal ionization mass spectrometry (TIMS) techniques on VG Instruments Sector 54-E multicollector mass spectrometers. The Pb isotopic compositions of three Jarigole picrites were reanalyzed at San Diego State University by multi-collector (MC)-ICP-MS using a Nu Plasma system. Sample powders were leached prior to analysis with dilute HBr. Isotopic values of standards were corrected using the Tl-doping technique (White *et al.*, 2000; Thirlwall 2002; Albarède *et al.*, 2004). Sample isotope ratios were corrected for within-run fractionation using standard–sample–standard bracketing techniques. The higher precision MC-ICP-MS data (Table 2) plotted in the figures confirm the HIMU-like nature of the Jarigole picrites (see Appendix for details).

Hand-picked olivine separates from three Jarigole picrites were analyzed for $^3\text{He}/^4\text{He}$ isotope compositions by D. Graham at Oregon State University (Table 2). Precise $^{40}\text{Ar}/^{39}\text{Ar}$ age determinations on three bulk-rock samples from Longipi and Kajong were obtained by R. Duncan at Oregon State University; weighted-mean plateau ages are reported in Table 3.

RESULTS

Major elements

Samples analyzed in this study include some of the most primitive lavas reported from eastern Africa. Mafic lavas with >8 wt % MgO are found at all study locations, although these same centers also produced more evolved lavas, including phonolites and rhyolites. Tertiary

Table 1: Major and trace element geochemistry

Sample:	LGP 607	LGP 207	LGP 36	LGP 04	LGP 39	LGP 12	KL 18	KL 02	KL 16	KL 13b	KL 14B	KL 06	LYG86 11	EST84 07	EST 7	EST 5
Locality:	Longipi	Longipi	Longipi	Longipi	Longipi	Longipi	Mt. Kulal	Mt. Kulal	Mt. Kulal	Mt. Kulal	Mt. Kulal	Mt. Kulal	Loiyangalani	Allia Bay	Allia Bay	Allia Bay
Age (Ma):*	1-5	3-5	1.5-3.5	1.5-3.5	1.5-3.5	1.5-3.5	~3	~3	~3	~3	~3	~3	~15	~15	~15	~15
SiO ₂	42.48	43.38	42.86	44.41	45.79	48.40	46.37	46.39	46.92	45.74	47.57	49.39	46.06	49.32	49.70	48.83
TiO ₂	2.80	2.91	2.67	2.45	2.33	2.16	2.07	2.02	2.67	2.45	2.61	2.78	2.50	2.74	2.65	2.67
Al ₂ O ₃	12.79	13.59	13.28	14.24	14.38	15.24	15.27	19.92	17.53	18.46	18.94	17.58	18.62	14.61	14.01	13.48
Fe ₂ O ₃	13.78	13.10	12.68	11.70	11.96	13.40	12.81	10.89	14.26	13.29	14.03	13.19	12.50	13.37	12.99	12.57
MgO	12.08	12.00	11.48	11.26	10.17	6.26	7.31	3.86	3.82	3.17	3.05	3.01	4.45	5.48	5.36	5.85
MnO	0.23	0.20	0.21	0.20	0.20	0.22	0.20	0.17	0.20	0.17	0.17	0.22	0.18	0.15	0.14	0.16
CaO	11.80	10.44	11.37	13.04	10.34	10.18	11.54	12.35	10.33	11.95	9.53	7.64	11.02	10.07	9.79	9.02
Na ₂ O	3.04	3.22	3.01	1.77	3.48	3.72	2.92	2.98	3.40	3.13	3.39	4.24	3.12	3.50	3.40	5.34
K ₂ O	1.46	1.92	1.92	1.38	1.78	0.90	1.33	1.05	1.37	1.17	1.36	2.17	1.08	1.59	1.10	1.64
P ₂ O ₅	0.66	0.56	0.63	0.45	0.56	0.37	0.43	0.33	0.45	0.37	0.44	0.76	0.44	0.44	0.42	0.40
Total	101.09	101.33	100.08	100.89	101.00	100.84	100.26	99.94	100.95	99.89	100.47	100.96	99.96	101.26	99.56	99.97
LOI	2.6	-0.1	1.0	2.4	0.1	1.3	1.8	1.6	2.8	3.6	2.5	2.5	1.5	1.9	1.5	4.4
Cs	0.45	0.30	0.39	0.15	0.37	0.20	0.06	0.13	0.19	0.16	0.21	0.22	0.19	0.08	0.06	—
Rb	20.2	35.4	38.8	20.7	32.3	18.8	11.2	15.8	20.8	17.7	21.8	38.4	22.9	22.5	21.4	—
Ba	545	470	531	704	499	407	412	359	323	287	324	578	322	408	381	—
Sr	658	547	690	923	579	370	560	616	535	545	550	578	644	567	552	—
Th	5.5	4.8	6.0	3.7	5.0	3.3	1.9	2.7	3.4	2.8	3.5	6.3	3.8	4.2	1.5	—
U	1.5	1.2	1.2	0.9	1.2	0.7	0.4	0.5	0.7	0.6	0.8	1.4	1.0	0.9	0.7	—
Pb	2.7	3.3	3.2	1.9	2.9	2.7	1.6	1.2	1.6	1.5	1.8	2.3	1.8	2.8	3.5	—
Ta	4.5	3.7	4.6	3.0	3.6	1.9	1.3	2.1	2.7	2.3	2.7	5.0	2.7	2.5	3.0	—
Nb	73.5	62.4	76.6	50.0	61.3	32.4	22.5	33.9	43.0	36.4	43.8	83.3	45.6	42.8	44.6	—
Hf	5.2	5.4	5.1	4.4	4.5	3.9	2.8	3.0	4.5	3.8	4.3	6.3	4.7	5.5	3.6	—
Zr	197	207	202	172	180	147	104	126	178	153	178	277	193	214	224	—
Y	30.2	32.0	28.6	28.4	29.5	33.1	27.1	21.3	30.8	26.3	33.3	40.8	28.4	28.4	28.1	—
Cr	463	473	484	346	400	88	120	46	32	36	35	9	47	44	41	—
Ni	211	231	206	175	163	75	91	57	46	51	43	26	54	76	70	—
Sc	29.2	30.0	27.8	34.4	28.6	35.2	39.2	21.3	24.5	25.1	24.6	16.4	22.7	29.3	29.9	—
V	238	240	233	263	231	293	300	237	279	292	289	102	247	291	304	—
La	46.0	39.1	46.2	31.4	41.8	30.2	23.6	22.2	28.9	24.3	30.2	51.6	30.2	37.5	33.7	—
Ce	90.1	78.9	89.8	65.1	83.1	63.6	50.6	44.6	60.5	50.5	60.3	102.1	60.9	79.3	69.9	—
Nd	40.3	36.6	39.5	30.7	36.7	30.7	26.2	21.0	29.6	25.1	30.0	45.5	28.7	38.0	34.5	—
Sm	8.30	7.78	7.99	6.67	7.35	6.50	5.75	4.52	6.43	5.59	6.61	9.21	6.07	7.92	7.14	—
Eu	2.64	2.50	2.54	2.24	2.33	2.25	2.02	1.61	2.12	1.90	2.18	2.90	2.04	2.47	2.28	—
Tb	1.20	1.18	1.16	1.01	1.09	1.10	0.93	0.72	1.06	0.89	1.07	1.38	0.99	1.11	1.00	—
Yb	2.19	2.52	2.09	2.35	2.47	2.77	2.24	1.80	2.52	2.20	2.68	3.41	2.34	2.11	2.10	—
Lu	0.33	0.37	0.30	0.34	0.38	0.43	0.35	0.26	0.37	0.33	0.40	0.51	0.34	0.30	0.30	—

Table 1: Continued

Sample:	EST 4	EST 3	EST 2	EST 1	JRG 12	JRG 10	JRG 07	JRG 09	JRG 01	JRG 06	LOD 1	LOD 3	LOD 5	LOD 2	LOD 6	Porr 606	Porr 404
Locality:	Allia Bay	Allia Bay	Allia Bay	Allia Bay	Jarigole	Jarigole	Jarigole	Jarigole	Jarigole	Jarigole	Lodwar	Lodwar	Lodwar	Lodwar	Lodwar	Mt. Porr	Mt. Porr
Age (Ma):*	~15	~15	~15	~15	17-23	17-23	17-23	17-23	17-23	17-23	23-26	23-26	23-26	23-26	23-26	~35	~35
SiO ₂	53.33	50.09	50.21	48.09	42.49	43.90	45.51	45.77	50.11	51.54	45.88	47.04	47.40	50.33	50.42	43.62	44.07
TiO ₂	2.42	2.90	3.43	2.10	1.13	1.47	2.11	2.59	3.55	3.54	1.63	1.87	2.11	2.37	3.43	3.11	2.85
Al ₂ O ₃	13.93	15.76	13.52	10.21	5.44	7.84	11.00	14.60	13.59	13.75	7.83	9.26	10.56	14.14	13.20	13.30	16.35
Fe ₂ O ₃	12.17	12.25	14.37	12.83	14.60	13.78	13.88	15.23	15.17	14.34	13.64	13.26	13.22	12.82	14.63	13.94	10.09
MgO	4.25	4.52	4.08	11.15	28.65	22.37	14.34	6.33	4.64	3.93	19.79	15.02	12.61	5.35	4.42	8.59	8.50
MnO	0.16	0.24	0.22	0.18	0.23	0.21	0.20	0.22	0.21	0.21	0.19	0.18	0.18	0.16	0.21	0.23	0.17
CaO	8.64	7.92	8.39	10.99	6.10	9.13	10.85	11.85	8.58	8.57	8.63	9.41	9.51	9.86	8.26	12.67	10.84
Na ₂ O	1.64	4.01	3.15	2.32	1.33	1.39	2.10	2.82	3.26	3.41	1.50	2.18	2.35	3.17	3.22	3.51	4.63
K ₂ O	3.06	1.51	1.09	0.82	0.44	0.59	0.86	0.97	0.92	1.34	0.47	0.70	0.73	1.09	1.01	1.11	2.03
P ₂ O ₅	0.40	0.59	0.60	0.32	0.17	0.22	0.32	0.37	0.54	0.67	0.23	0.24	0.30	0.40	0.58	0.72	0.29
Total	99.99	99.79	99.07	99.01	100.59	100.91	101.16	100.74	100.56	101.30	99.78	99.15	98.99	99.68	99.38	100.79	99.82
LOI	7.9	2.4	4.2	2.2	0.9	1.5	1.2	0.3	1.2	1.1	2.3	1.0	1.8	2.8	0.5	1.1	4.0
Cs	0.08	—	—	0.11	0.20	0.18	0.20	0.32	0.22	0.30	0.12	0.08	0.13	—	0.17	0.30	0.79
Rb	46.3	—	—	16.7	7.0	7.2	13.7	14.9	16.9	20.4	7.9	13.2	17.1	—	25.1	32.0	65.3
Ba	633	—	—	299	90	107	174	195	302	315	126	205	255	—	359	460	961
Sr	173	—	—	417	179	198	318	400	355	361	251	318	394	—	407	667	730
Th	1.3	—	—	3.3	1.3	1.6	2.5	2.9	3.0	3.2	1.9	2.6	3.3	—	3.5	8.7	5.3
U	0.3	—	—	0.7	0.3	0.4	0.6	0.8	0.8	0.8	0.4	0.6	0.8	—	0.9	2.3	1.2
Pb	4.4	—	—	4.1	1.0	1.2	2.6	2.4	3.7	3.8	1.6	2.9	3.1	—	4.1	4.2	3.6
Ta	2.3	—	—	2.7	0.9	1.1	1.7	2.0	2.0	2.2	1.6	2.1	2.5	—	2.7	6.2	4.4
Nb	38.3	—	—	36.5	14.7	17.4	27.7	32.3	32.8	34.7	21.9	41.3	35.6	—	40.8	101.0	73.8
Hf	2.9	—	—	4.3	2.1	2.6	3.7	4.6	6.7	6.9	3.7	3.7	4.6	—	8.1	6.4	4.6
Zr	184	—	—	173	79	100	139	175	252	262	148	148	182	—	324	252	174
Y	25.6	—	—	23.1	12.4	15.9	21.8	28.6	47.9	49.6	16.5	19.6	24.6	—	57.0	31.4	22.5
Cr	18	—	—	670	1845	768	399	54	14	10	1217	781	545	—	7	242	169
Ni	48	—	—	262	902	620	334	93	40	36	685	410	373	—	33	124	128
Sc	20.6	—	—	30.6	21.7	29.6	28.9	28.8	32.5	33.6	28.1	26.0	28.1	—	35.7	31.4	30.6
V	183	—	—	244	150	185	249	309	390	338	228	212	255	—	444	280	290
La	29.3	—	—	30.2	11.4	14.2	22.4	26.1	29.6	31.2	16.4	22.4	28.8	—	35.6	71.1	39.7
Ce	61.1	—	—	63.1	24.9	31.4	48.1	56.7	68.0	72.4	34.9	47.8	61.2	—	83.0	141.7	79.7
Nd	29.6	—	—	29.6	13.1	16.1	23.9	29.1	38.6	40.7	19.6	22.9	29.1	—	46.0	58.8	28.1
Sm	6.06	—	—	6.21	2.93	3.70	5.35	6.54	9.33	9.79	4.23	4.98	6.36	—	11.15	10.67	6.52
Eu	1.93	—	—	1.89	0.91	1.18	1.72	2.09	2.85	2.95	1.30	1.47	1.90	—	3.32	3.15	2.16
Tb	0.88	—	—	0.93	0.46	0.60	0.82	1.03	1.56	1.64	0.64	0.76	0.92	—	1.85	1.34	0.89
Yb	1.93	—	—	1.71	0.93	1.22	1.74	2.24	3.98	4.15	1.32	1.40	1.92	—	5.21	2.45	1.81
Lu	0.29	—	—	0.25	0.14	0.19	0.24	0.33	0.59	0.63	0.19	0.22	0.27	—	0.65	0.33	0.27

Sample:	Porr 4		Porr 602		Porr 2		Porr 3		Porr 5		Porr 407		Porr 7		Porr 604		Porr 6		KJ 16		KJ 1		KJ 2		KJ 13		KJ 19		KJ 18	
	Mt.	Porr	Mt.	Porr	Mt.	Porr	Mt.	Porr	Mt.	Porr	Mt.	Porr	Mt.	Porr	Mt.	Porr	Mt.	Porr	Mt.	Porr	Mt.	Porr	Mt.	Porr	Mt.	Porr	Mt.	Porr	Mt.	Porr
Locality:	~35	~35	~35	~35	~35	~35	~35	~35	~35	~35	~35	~35	~35	~35	~35	~35	~35	~35	~35	~35	~35	~35	~35	~35	~35	~35	~35	~35	~35	~35
Age (Ma):*	~35	~35	~35	~35	~35	~35	~35	~35	~35	~35	~35	~35	~35	~35	~35	~35	~35	~35	~35	~35	~35	~35	~35	~35	~35	~35	~35	~35	~35	~35
SiO ₂	45-62	44-87	46-07	45-86	45-56	47-59	49-37	50-14	50-44	47-11	40-78	47-05	39-63	47-97	50-41															
TiO ₂	2-78	2-77	2-62	2-72	2-68	2-44	2-30	3-40	3-38	2-70	3-34	1-95	4-02	2-27	3-23															
Al ₂ O ₃	15-71	16-75	16-11	15-98	15-81	15-22	14-21	13-50	13-28	12-19	13-28	15-57	14-24	15-07	13-99															
Fe ₂ O ₃	9-88	9-91	9-66	9-70	9-57	13-84	13-20	14-50	14-52	10-13	13-87	12-60	15-41	13-58	14-61															
MgO	8-37	7-97	7-95	7-83	7-74	5-97	5-82	4-52	4-36	9-54	8-08	7-10	6-45	6-05	4-95															
MnO	0-16	0-17	0-16	0-16	0-16	0-18	0-20	0-21	0-23	0-20	0-22	0-19	0-29	0-22	0-21															
CaO	10-70	10-57	10-38	10-51	10-45	10-31	9-84	8-23	8-20	13-43	13-13	12-62	13-67	9-60	8-80															
Na ₂ O	4-46	5-31	4-81	4-97	5-20	3-14	3-17	3-41	3-26	3-26	5-11	2-55	4-98	3-40	3-31															
K ₂ O	1-62	1-67	1-93	1-50	1-11	1-06	0-70	0-90	1-00	1-58	0-83	0-82	1-13	1-07	1-12															
P ₂ O ₅	0-25	0-29	0-26	0-28	0-34	0-31	0-30	0-57	0-63	0-78	0-55	0-38	1-51	0-43	0-50															
Total	99-55	100-28	99-95	99-52	98-61	100-06	99-10	99-39	99-30	100-92	99-21	100-84	101-31	99-66	101-13															
LOI	3-8	3-9	4-6	3-3	3-5	1-8	1-5	0-4	-0-1	7-1	4-1	0-9	1-9	2-7	1-8															
Cs	0-77	0-78	0-82	0-78	0-88	0-04	-	0-34	0-26	0-38	0-76	0-08	0-64	0-12	0-25															
Rb	64-7	20-2	69-1	41-0	49-7	3-2	-	22-6	18-6	13-7	8-4	10-9	46-9	19-4	17-6															
Ba	944	975	932	924	958	354	-	319	343	1068	765	1066	684	430	294															
Sr	747	536	617	601	624	380	-	361	346	842	896	492	901	450	399															
Th	5-1	5-5	5-9	5-5	5-7	2-5	-	3-3	2-9	7-9	17-9	2-2	13-2	3-5	3-0															
U	1-3	1-2	1-3	1-3	1-3	0-2	-	1-0	0-7	2-1	1-6	0-4	3-3	0-6	0-8															
Pb	3-1	3-2	3-6	3-3	4-1	3-5	-	3-6	4-0	5-8	3-7	1-4	5-3	2-8	3-6															
Ta	5-2	4-8	6-3	6-2	5-5	1-4	-	2-1	2-5	5-3	8-0	1-2	9-0	2-0	2-0															
Nb	75-0	77-2	79-3	77-5	80-0	22-4	-	35-7	33-7	91-1	150-7	21-3	147-5	34-6	32-3															
Hf	4-5	4-9	4-8	4-8	5-0	5-4	-	6-9	7-0	5-7	6-3	2-7	9-9	4-1	6-6															
Zr	176	186	192	185	198	198	-	258	272	226	277	100	415	157	246															
Y	21-7	22-9	22-1	21-8	23-1	37-5	-	48-5	47-5	29-4	33-4	26-2	46-7	35-1	44-5															
Cr	150	144	149	128	150	61	-	12	6	449	118	215	36	70	38															
Ni	132	112	119	113	105	58	-	36	27	155	83	113	60	71	51															
Sc	28-7	29-9	25-7	26-7	27-8	36-7	-	30-9	28-6	32-3	35-7	36-2	21-5	34-3	34-3															
V	299	279	266	299	276	216	-	349	347	254	333	281	269	295	378															
La	37-5	41-6	39-7	38-9	43-0	21-1	-	31-2	39-7	61-9	92-0	20-3	120-1	33-3	29-2															
Ce	72-8	83-0	76-3	74-8	85-6	48-7	-	71-7	77-6	121-4	175-7	42-6	242-5	69-1	67-2															
Nd	34-6	34-8	35-4	35-1	36-1	27-8	-	39-8	38-6	53-2	67-4	22-5	102-2	33-7	37-4															
Sm	6-39	6-66	6-50	6-45	6-72	6-82	-	9-49	9-24	9-94	11-28	5-03	17-76	7-18	8-85															
Eu	1-87	2-23	1-89	1-90	2-10	2-15	-	2-91	2-75	3-13	3-34	2-02	5-04	2-40	2-67															
Tb	0-83	0-90	0-71	0-82	0-91	1-21	-	1-60	1-61	1-26	1-44	0-86	2-16	1-47	1-47															
Yb	1-71	1-93	1-75	1-75	1-94	3-19	-	4-06	4-22	2-24	2-49	2-20	3-33	2-94	3-69															
Lu	0-25	0-28	0-28	0-27	0-28	0-46	-	0-59	0-55	0-33	0-35	0-32	0-47	0-45	0-55															

*Ages of volcanism from Ochieng' *et al.* (1988) except for LGP 607, LGP 207, KJ 16. M. Rudnicki and G. Dwyer, analysts. Precision based on replicate analyses of samples and natural basalt standards is generally <1% for SiO₂, Sr, Y, Zr, Nb, La and Ce; <3% for other major elements, Ba, Sr, Rb, Cs, Cr, Sc, V, Co, Pr, Nd, Sm, Eu, Gd, Tb, Dy, Ho, Er and Hf; <5% for Ni, Yb, Lu, Pb, Th and Ta; and <8% for U.

Table 2: Isotopic data

Measured values								
Sample	Age (Ma)*	$^{87}\text{Sr}/^{86}\text{Sr}$	$^{143}\text{Nd}/^{144}\text{Nd}$	ϵNd	$^{206}\text{Pb}/^{204}\text{Pb}$	$^{207}\text{Pb}/^{204}\text{Pb}$	$^{208}\text{Pb}/^{204}\text{Pb}$	$^3\text{He}/^4\text{He}\dagger$
LGP 607	1.5 + 0.2	0.703183	0.512927	5.6	19.375	15.691	39.290	
LGP 36	2.5	0.703295	0.512904	5.2	19.316	15.617	39.158	
LGP 4	2.5	0.704230	0.512895	5.0	19.308	15.630	39.166	
LGP 39	2.5	0.703352	0.512872	4.6	19.274	15.613	39.089	
KL 18	3	0.704719	0.512671	0.6	19.820	15.777	39.757	
LGP 207	3.5 + 0.3	0.703231	0.512911	5.3				
JRG 12	20	0.703231	0.512772	2.6	20.216	15.728	39.890	6.15 + 0.27
JRG 10	20	0.703119	0.512838	3.9	20.176	15.712	39.803	6.59 + 0.25
JRG 7	20	0.703279	0.512828	3.7	20.226	15.731	39.803	6.26 + 0.23
JRG 12 (SDSU)‡					20.454	15.740	40.094	
JRG 10 (SDSU)					20.254	15.704	39.850	
JRG 7 (SDSU)					20.385	15.718	39.985	
Porr 606	35	0.703151	0.512802	3.2	20.436	15.703	39.998	
Porr 404	35	0.703470	0.512839	3.9	20.123	15.762	40.087	
Porr 602	35	0.703407	0.512837	3.9	20.066	15.669	39.878	
KJ 1	39	0.703275	0.512785	2.9	20.238	15.731	39.998	
KJ 16	39.2 + 0.4	0.703463	0.512862	4.4	18.903	15.602	38.707	
Age-corrected values								
Sample	Age (Ma)	$(^{87}\text{Sr}/^{86}\text{Sr})_i$	$(^{143}\text{Nd}/^{144}\text{Nd})_i$	ϵNd_i	$(^{206}\text{Pb}/^{204}\text{Pb})_i$	$(^{207}\text{Pb}/^{204}\text{Pb})_i$	$(^{208}\text{Pb}/^{204}\text{Pb})_i$	
LGP 607	1.5 + 0.2	0.703180	0.512925	5.7	19.36	15.69	39.27	
LGP 36	2.5	0.703289	0.512902	5.2	19.31	15.62	39.14	
LGP 4	2.5	0.704228	0.512893	5.0	19.29	15.63	39.15	
LGP 39	2.5	0.703346	0.512870	4.6	19.26	15.61	39.07	
KL 18	3	0.704717	0.512668	0.7	19.81	15.78	39.74	
LGP 207	3.5 + 0.3	0.703224	0.512909	5.3				
JRG 12	20	0.703200	0.512754	2.8	20.14	15.72	39.80	
JRG 10	20	0.703090	0.512819	4.0	20.11	15.71	39.71	
JRG 7	20	0.703244	0.512810	3.8	20.17	15.73	39.74	
JRG 12 (SDSU)					20.38	15.73	40.00	
JRG 10 (SDSU)					20.19	15.70	39.76	
JRG 7 (SDSU)					20.33	15.72	39.92	
Porr 606	35	0.703084	0.512776	3.6	20.33	15.70	39.74	
Porr 404	35	0.703344	0.512806	4.1	19.99	15.76	39.91	
Porr 602	35	0.703354	0.512809	4.2	19.93	15.66	39.67	
KJ 1	39	0.703260	0.512758	3.3	20.06	15.72	39.34	
KJ 16	39.2 + 0.4	0.703437	0.512832	4.8	18.75	15.60	38.52	

*Ages used for correction as estimated from Ochieng' *et al.* (1988), except for LGP 607, LGP 207 and KJ 16.

†Values reported as R/R_A; measurements made on olivine.

‡Analysis of leached chips performed at San Diego State University.

Turkana lavas reported here are primarily basaltic and basaltic, based on the silica-alkali classification scheme (Fig. 2). The 39–35 Ma lavas from Mt. Porr and Kajong and 3.5–1.5 Ma lavas from Longipi extend to basaltic compositions; picrites are found at Jarigole (23–17 Ma).

Both the oldest and youngest suites are dominated by nepheline-normative compositions, whereas the intermediate volcanic period is represented by nepheline-, hypersthene- and quartz-normative lavas (Fig. 2). Accumulative olivine in select Jarigole and Lodwar samples is manifest in high normative olivine contents.

Table 3. $^{40}\text{Ar}/^{39}\text{Ar}$ age data

Sample	$^{40}\text{Ar}/^{39}\text{Ar}$	Heating steps	Ar fraction (%)	MSWD
KJ 16	39.19 + 0.39	5-step plateau	51.8	2.30
LGP 607	1.50 + 0.19	4-step plateau	75.9	1.95
LGP 207	3.50 + 0.27	7-step plateau	94.3	1.14

Group A Kajong lavas (39 Ma) have high normative nepheline contents that correlate with high loss-on-ignition values (LOI; Table 1); no correlation is found among the nepheline-normative Mt. Kulal and Longipi lavas (3.5–1.5 Ma).

The highly evolved nature of many Tertiary Turkana samples indicates an important role for fractionation. However, it is clear that fractional crystallization alone cannot explain many geochemical features of the mafic Tertiary samples. Major element oxides (Al_2O_3 , TiO_2 , P_2O_5 and $\text{CaO}/\text{Al}_2\text{O}_3$) show essentially no correlation with MgO among the non-accumulative ($\text{MgO} \leq 15$ wt %; Fig. 3) Jarigole and Lodwar series (Fig. 3). Basanite lavas from Mt. Porr, Kajong and Longipi have anomalously high contents of K_2O , resulting in high normative nepheline values (17–24 %), and are also enriched in TiO_2 and P_2O_5 . These geochemical features suggest a genesis distinct from that of the majority of the less alkaline samples investigated (Fig. 3). Most of the youngest Tertiary lavas have major element compositions that overlap Quaternary Turkana lavas (Furman *et al.*, 2004).

Trace elements

Compatible trace elements

Several Tertiary Turkana samples with 8–12 wt % MgO have undergone little fractionation since initially forming as partial melts from the mantle. These primitive samples contain up to ~350 ppm Ni, ~450 ppm Cr and 35 ppm Sc, indicating only minor removal of olivine and/or clinopyroxene from primary mantle melts, and are thus important for interpreting source components in Turkana magmatism. Jarigole and Lodwar picrites with 12.9–28.8 wt % MgO have up to ~900 ppm Ni, indicating accumulation of olivine phenocrysts (Fig. 3).

Incompatible trace elements

Tertiary Turkana lavas are broadly enriched in highly incompatible trace elements with respect to the primitive mantle (Fig. 4). All of the samples are characterized by positive Nb and negative K anomalies; selected samples display marked positive Ba anomalies and/or rare earth element (REE) enrichment relative to the high field strength elements Zr and Ti. Individual trace element

abundances generally correlate negatively with MgO among the Tertiary Turkana lavas, although variations between and within suites preclude their derivation from a common and homogeneous source.

Successive generations of Turkana lavas have distinctive trace element abundance patterns. The oldest basanites from Kajong and Mt. Porr have the highest degree of incompatible trace element enrichment observed, whereas Jarigole and Lodwar basalts and picrites show the least enrichment over primitive mantle. Latest Tertiary to Quaternary mafic lavas tend to have trace element abundances intermediate to those measured in the oldest two series of Turkana basalts.

Basalt and picrites from Jarigole and Lodwar have a restricted range in incompatible trace element abundances that indicate derivation from a sub-lithospheric mantle source region. Their Ba/Nb–La/Nb values overlap those of HIMU ocean island basalts (Chaffey *et al.*, 1989; Sun & McDonough, 1989), and their Ce/Pb–Nb/U and Ba/Rb–Rb/Sr values are characteristic of global basalts derived from anhydrous mantle source regions (Fig. 4). Most Tertiary and Quaternary Turkana samples also have incompatible trace element ratios within the ranges of mid-ocean ridge and HIMU basalts (Fig. 4), although a small number of lavas (KJ 2, KJ 19, LGP 12, KL 18) plot amongst the suite of 35–45 Ma mafic lavas from southern Ethiopia (Stewart & Rogers, 1996; George & Rogers, 2002) and define a trend towards an EM1-like component or enriched mantle lithosphere.

Variations in incompatible trace element abundances provide useful constraints on the accessory phase mineralogy of potential mantle source regions for primitive Turkana mafic lavas. For example, high Ba/Rb and low values of K/Nb and K/La suggest melting of amphibole-bearing material in the source region of Group A Kajong lavas (KJ 1, KJ 13 and KJ 16; Fig. 4); a lack of correlation between these parameters and LOI values suggests that they are a feature of the source region rather than of post-eruption hydrous alteration. A minor role for carbonatite metasomatism is indicated by the extreme Ba enrichment and relative negative Zr–Hf–Ti anomalies in the entire Kajong suite and in selected Mt. Porr lavas (e.g. Yaxley *et al.*, 1991). In contrast, there is no evidence to suggest that phlogopite or oxide phases (ilmenite, rutile) control the minor and trace element chemistry of the Tertiary Turkana mafic rocks.

Rare earth elements

Chondrite-normalized REE patterns appear smooth with negative, shallow slopes; Eu anomalies are generally absent. Samples from individual localities—excluding Kajong—have parallel patterns that typically do not cross. Group A Kajong samples, interpreted as melts

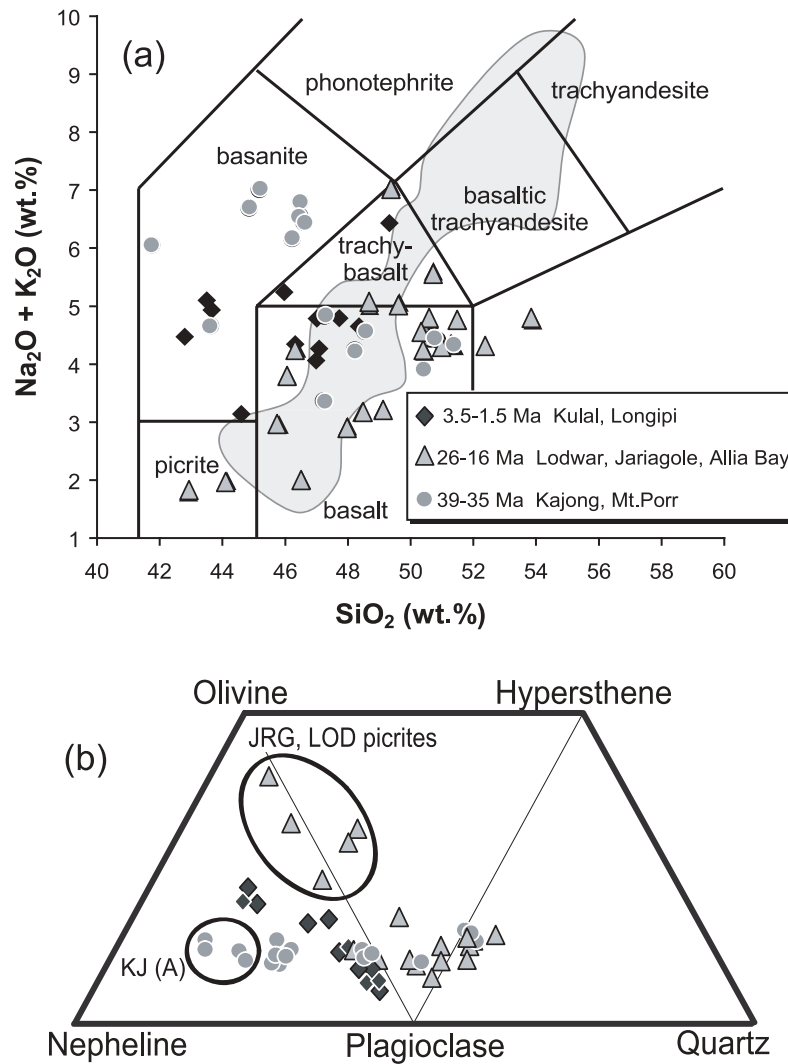


Fig. 2. Classification and nomenclature of Turkana lavas. (a) Total alkalis (Na₂O + K₂O wt %) vs SiO₂ variations in Turkana lavas [igneous rock classification from Le Maitre (1976)]. Shaded field of Quaternary Turkana data is from Furman *et al.* (2004). (b) Normative compositions of Turkana mafic lavas. Symbols as in (a). Field labeled KJ(A) encloses Kajong Group A lavas; field labeled JRG, LOD picrites encloses mafic lavas from Jariagole and Lodwar with ≥ 14.3 wt % MgO.

of an amphibole-bearing source, have weakly concave-upwards patterns (Fig. 5), reflecting the greater compatibility of the middle REE (MREE) in this phase (e.g. Zack *et al.*, 1997). The REE patterns of these samples mimic those of lithosphere-derived samples from Bird Nest Island (Fig. 5; Furman *et al.*, 2004). Anomalously high light REE (LREE) abundances in Group A Kajong lavas (Fig. 5) may be associated with carbonatite metasomatism (e.g. Yaxley *et al.*, 1991; Rudnick *et al.*, 1993).

Tertiary Turkana samples have consistently higher Tb/Yb_n values [the subscript n indicates values normalized to the chondritic abundances of Boynton (1984)] than the Quaternary suite (Fig. 5). The Tertiary values are within the range measured on basalts from throughout the Kenya Rift (Macdonald *et al.*, 2001) although

they do not extend to values as high as those observed in the Chyulu Hills, southern Kenya, where the crustal thickness exceeds 100 km (Späth *et al.*, 2001).

Isotope data

Precise ⁴⁰Ar/³⁹Ar age determinations were made on three whole-rock samples from Kajong and Longipi (Table 3). Kajong lava KJ 16 (39.2 ± 0.4 Ma) is the oldest volcanic sample dated from the Turkana region (Walsh & Dodson, 1969; Zanettin *et al.*, 1983; Ochieng' *et al.*, 1988; Morley *et al.*, 1992; Hendrie *et al.*, 1994). Longipi basanite samples LGP 607 and LGP 207 are the first from this area to be dated, and indicate activity at this volcanic center between 3.5 and 1.5 Ma.

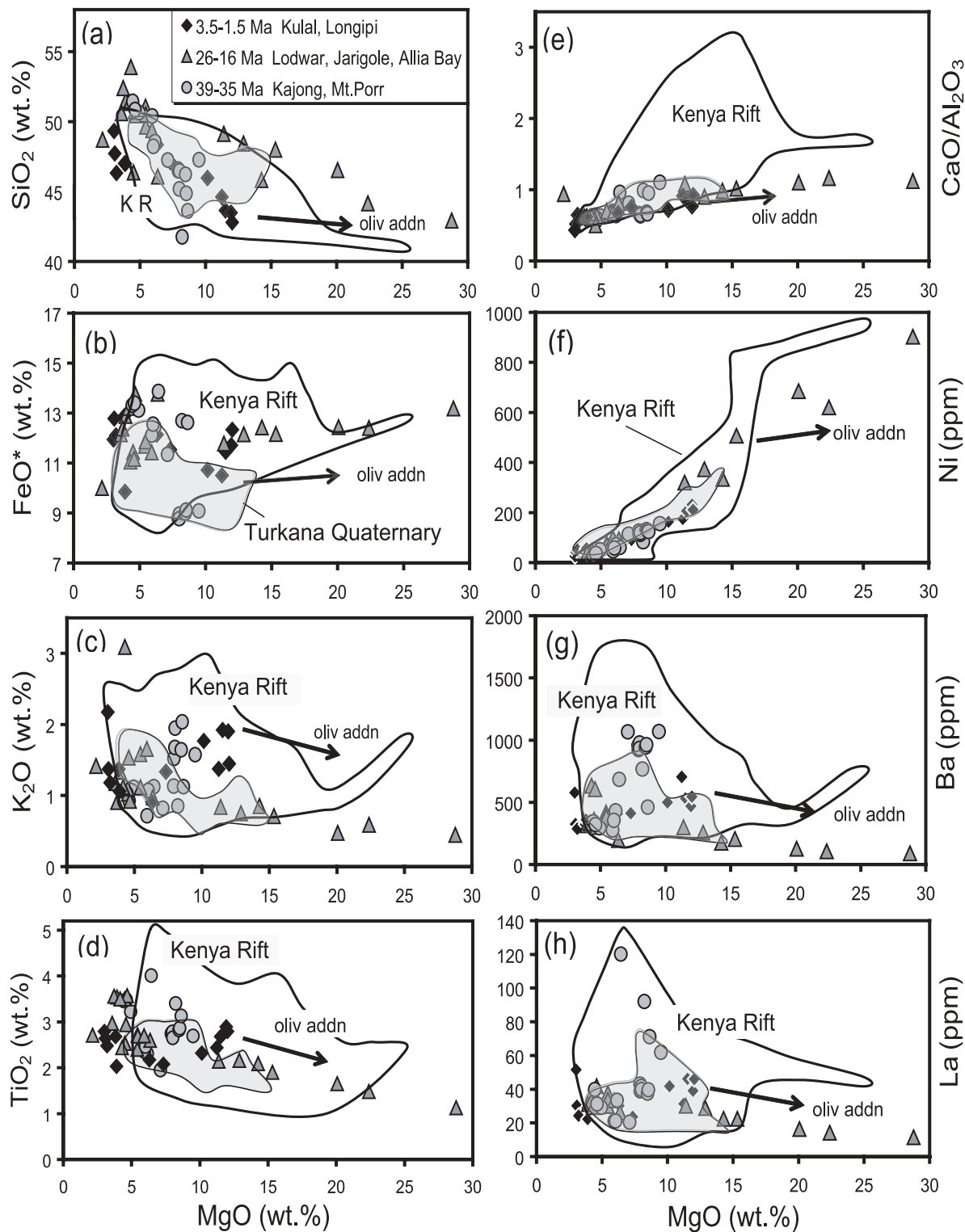


Fig. 3. Whole-rock geochemical characteristics of Turkana lavas as a function of wt % MgO. The effects of olivine addition are indicated by the labeled vector. The shaded fields encompass Quaternary Turkana mafic lavas (Furman *et al.*, 2004). Geochemical variations among basalts from portions of the Kenya Rift underlain by rifted margins and ancient cratons are shown by the open field (Macdonald *et al.*, 2001); this group includes samples for which continental crustal contamination can be demonstrated.

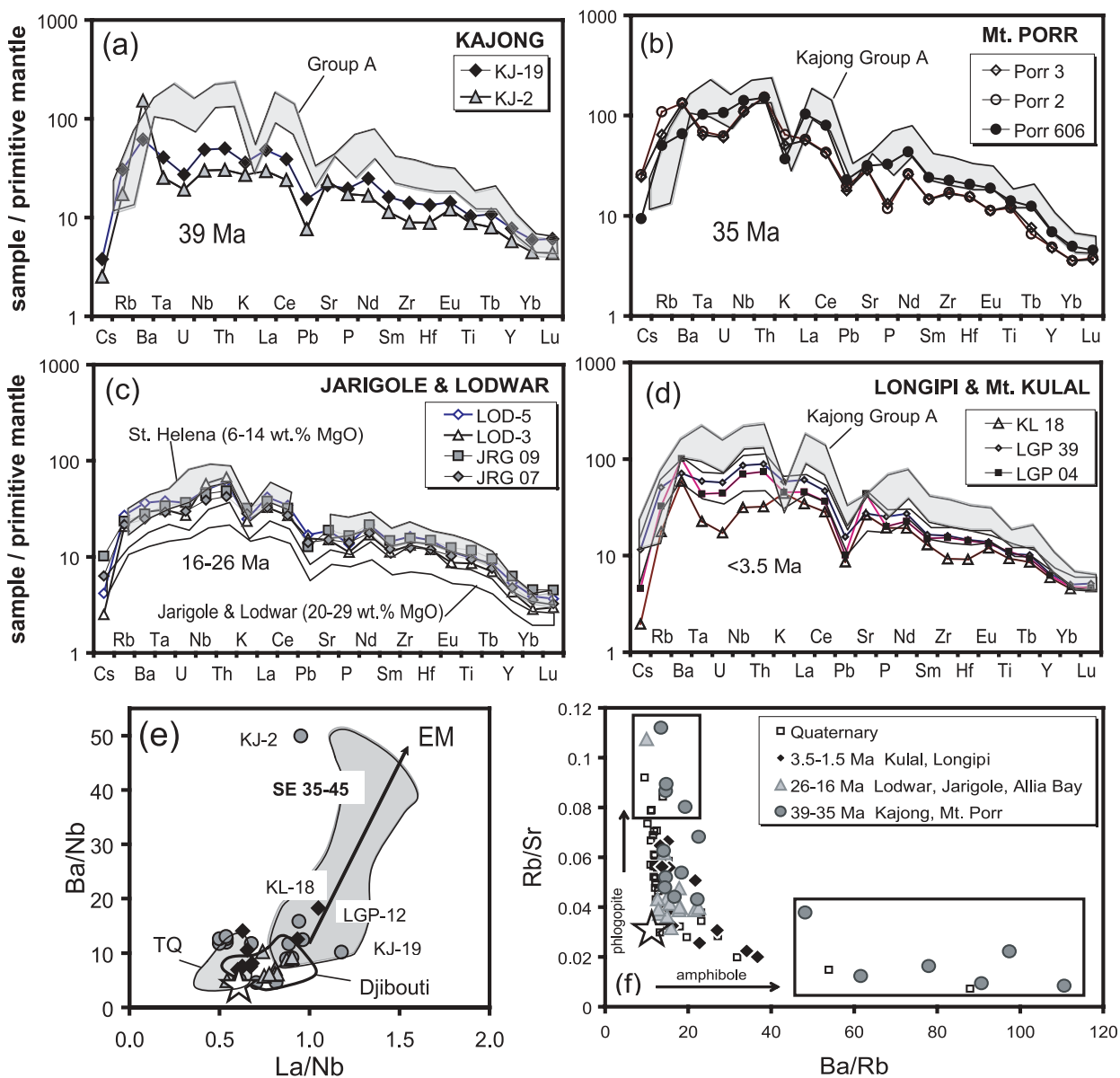


Fig. 4. (a–d) Primitive mantle-normalized incompatible trace element (ITE) variation diagrams for samples from different locations and time periods. (a) Kajong Group A and (b) Mt. Porr mafic lavas have the highest degree of ITE enrichment; negative K anomalies indicate melting in the presence of residual amphibole. (c) Jarigole and Lodwar basalts and picrites have the lowest degree of ITE enrichment; their patterns overlap HIMU basalts from St. Helena (Chaffey *et al.*, 1989). (d) Longipi and Kulal basalts have ITE contents intermediate to those of the older suites. (e) Tertiary Turkana La/Nb–Ba/Nb values cluster near those of HIMU basalts (represented by the star) and Quaternary Turkana mafic lavas (field labeled TQ), and are lower than those observed among <2 Ma basalts from Djibouti (the modern Afar plume; Deniel *et al.*, 1994). Kajong Group A, Kulal and Longipi lavas have high La/Nb–Ba/Nb values similar to 35–45 Ma basalts from southern Ethiopia (Stewart & Rogers, 1996; George & Rogers, 2002) that are characteristic of enriched mantle or mantle lithosphere sources (EM). (f) Ba/Rb–Rb/Sr variations in Turkana lavas indicate a limited role for amphibole (elevated Ba/Rb) and either phlogopite or carbonatite metasomatism (elevated Rb/Sr). Jarigole and Lodwar lavas fall within the range of HIMU basalts from St. Helena as indicated by the star (Chaffey *et al.*, 1989).

Radiogenic Sr–Nd–Pb isotope data for the Tertiary Turkana lavas (Fig. 6; Table 2) indicate substantial source heterogeneity, both within and between eruptive episodes. For example, the oldest basanites from Kajong and Mt. Porr have a narrow range of (⁸⁷Sr/⁸⁶Sr)_i values (0.70308–0.70344) but widely variable (²⁰⁶Pb/²⁰⁴Pb)_i

values (18.75–20.33). In contrast, Plio-Pleistocene lavas from Mt. Kulal and Longipi display the greatest variability in initial Sr isotope ratios (0.70318–0.70472) but define a much tighter range of initial ²⁰⁶Pb/²⁰⁴Pb values (19.26–19.81). Jarigole picrites and transitional basalts are more compositionally restricted, with Sr–Pb isotope

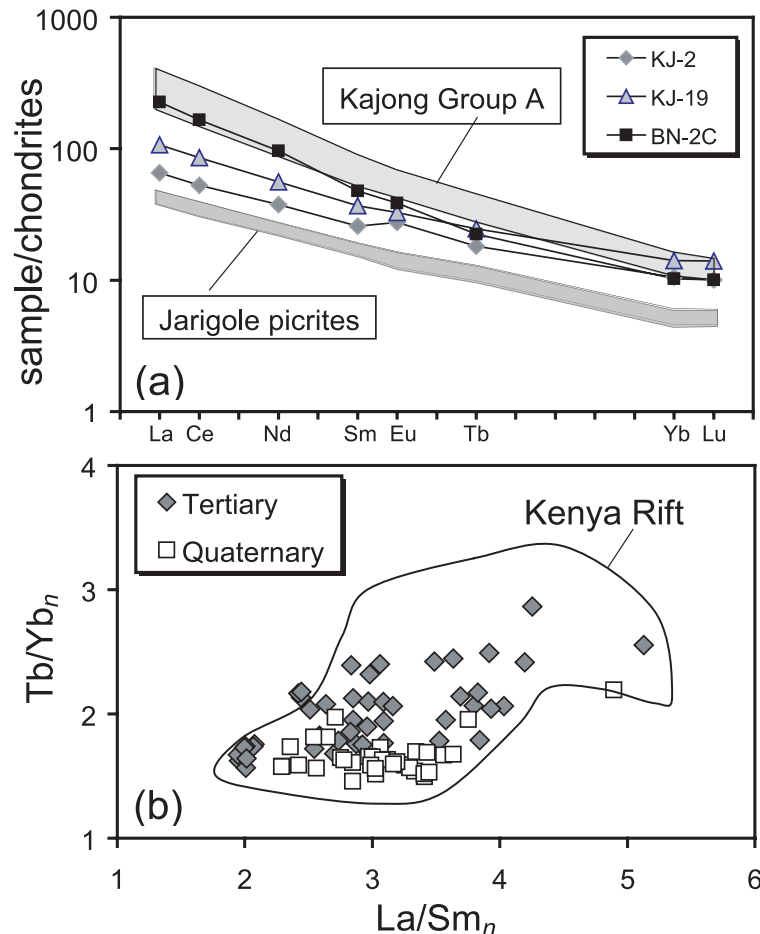


Fig. 5. (a) Chondrite-normalized REE patterns for Turkana mafic lavas. Kajong Group A samples (39 Ma) have patterns that match those of Quaternary basalts interpreted as melts of subcontinental lithospheric mantle (e.g. BN-2C; Furman *et al.*, 2004). (b) La/Sm_n - Tb/Yb_n variations in mafic lavas with >6 wt % MgO. The high values of Tb/Yb_n observed in Tertiary Turkana lavas and other portions of the Kenya Rift with moderately thick crust (Macdonald *et al.*, 2001; Späth *et al.*, 2001) suggest melting of enriched lithosphere in the presence of residual garnet (or clinopyroxene rich in Ca-Tschermak component; Blundy *et al.*, 1998).

values that are markedly similar to HIMU-like lavas from St. Helena and South Africa (Chaffey *et al.*, 1989; Janney *et al.*, 2002).

Initial $^{87}\text{Sr}/^{86}\text{Sr}$ ratios of mafic Tertiary Turkana rocks are among the lowest measured in the East African Rift; only two samples (LGP 4 and KL 18) have values >0.7035 . Many of the Tertiary samples have Sr–Nd isotope compositions that overlap those of Quaternary Turkana basalts (Fig. 6). Two Pliocene samples (KL 18 and LGP 4) have substantially higher $^{87}\text{Sr}/^{86}\text{Sr}$ and lower $^{143}\text{Nd}/^{144}\text{Nd}$, similar to values observed in selected Quaternary samples interpreted as lithospheric melts (Furman *et al.*, 2004) and falling within the ranges of both Recent and Miocene Ethiopian basalts (Stewart & Rogers, 1996; Furman *et al.*, 2006). When considered as a group, the Sr–Nd isotopic signatures of the Tertiary lavas broadly suggest mixing between a HIMU-like component and an enriched source component.

Tertiary Turkana lavas have highly variable radiogenic Pb isotope signatures with $^{206}\text{Pb}/^{204}\text{Pb}$ and $^{208}\text{Pb}/^{204}\text{Pb}$ extending to nearly the highest values of silicates documented in the African Rift (Fig. 6). The oldest lavas from Kajong and Mt. Porr span a wide range of $^{206}\text{Pb}/^{204}\text{Pb}$ values comparable with that observed in contemporaneous southern Ethiopian basalts (Stewart & Rogers, 1996). In contrast, early Miocene Jarigole picrites have consistently high $^{206}\text{Pb}/^{204}\text{Pb}$ and low $^{87}\text{Sr}/^{86}\text{Sr}$ values that fall on the edge of the field defined by HIMU basalts from St. Helena (Chaffey *et al.*, 1989) and in other African volcanic provinces (e.g. the Cameroon Line, Halliday *et al.*, 1988; the Western Cape melilitite province, Janney *et al.*, 2002). We refer to the Pb isotopic signatures of the Turkana lavas as high- μ (high U/Pb) and restrict use of the term HIMU to indicate the mantle end-member (e.g. Stracke *et al.*, 2005). The Pb isotope signatures of Pliocene to Quaternary Turkana lavas range

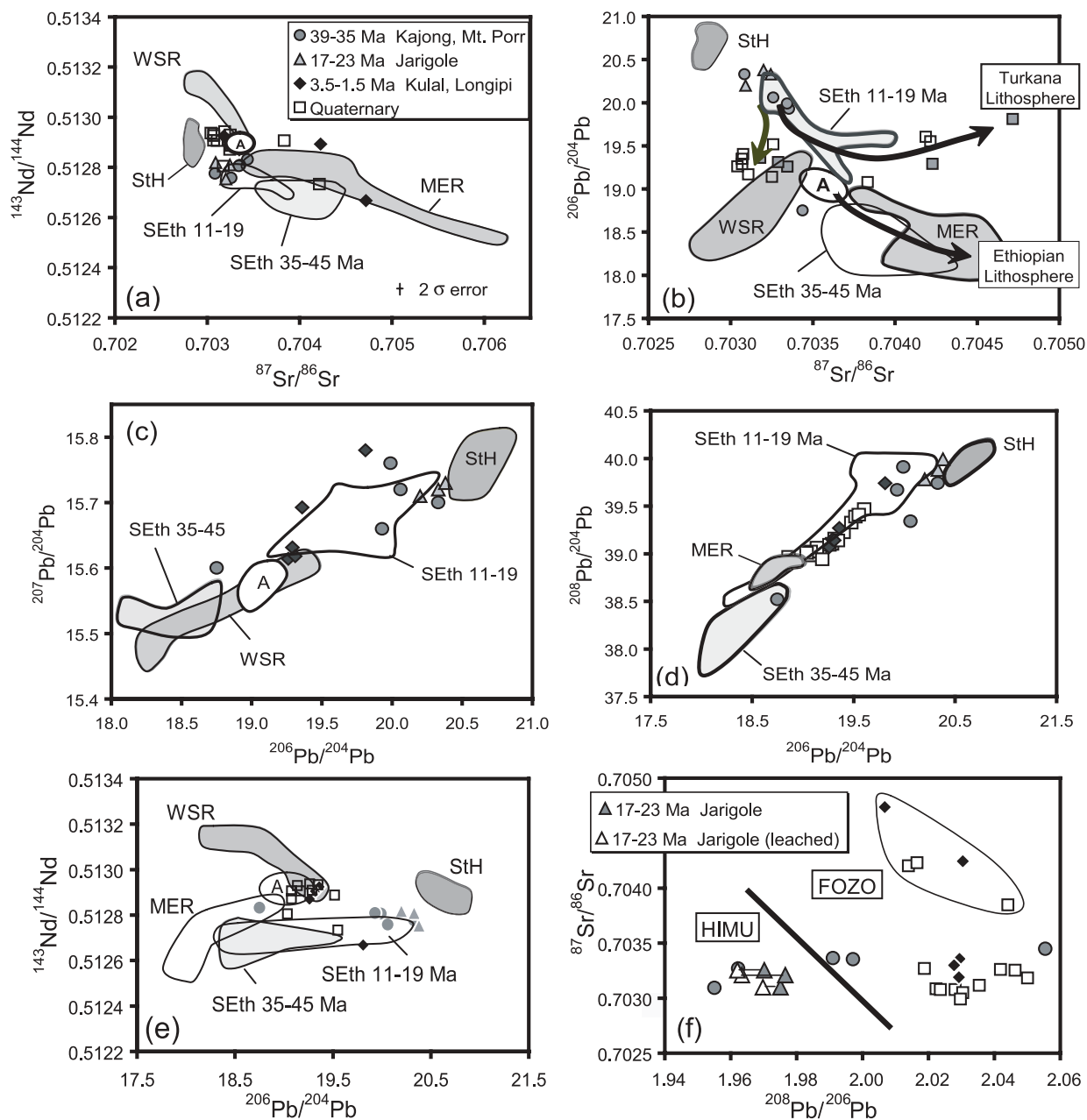


Fig. 6. Regional isotope variations along the EARS. (a) Sr–Nd isotope values in Tertiary Turkana samples are intermediate between those of Quaternary Turkana lavas (Furman *et al.*, 2004) and basalts of all ages from all the Ethiopian Rift. Turkana samples with $^{87}\text{Sr}/^{86}\text{Sr} > 0.7035$ are interpreted as melts of lithospheric mantle. MER, Main Ethiopian Rift (Trua *et al.*, 1999; Furman *et al.*, 2006); SEth, southern Ethiopia (Hart *et al.*, 1989; Stewart & Rogers, 1996; George & Rogers, 2002); StH, HIMU St. Helena basalts (Chaffey *et al.*, 1989); A, modern Afar plume (Deniel *et al.*, 1994; Schilling *et al.*, 1998); WSR, West Sheba Ridge (Schilling *et al.*, 1998). (b) Values of $^{87}\text{Sr}/^{86}\text{Sr}$ – $^{206}\text{Pb}/^{204}\text{Pb}$ in Jarigole picrites define a regional high- μ end-member. Most Turkana basalts record mixing between this high- μ end-member or the Afar plume with a more depleted mantle component. Southern Ethiopian basalts from 11 to 19 Ma and modern Main Ethiopian Rift lavas record involvement of ‘Ethiopian Lithosphere’, whereas southern Ethiopian basalts from 11 to 19 Ma and <3 Ma Turkana basalts sample ‘Turkana Lithosphere’. (c) A few Turkana lavas have high $^{207}\text{Pb}/^{204}\text{Pb}$ values at a given $^{206}\text{Pb}/^{204}\text{Pb}$, suggesting involvement of lithospheric mantle. This feature is also seen in selected Ethiopian lavas. (d) Values of $^{206}\text{Pb}/^{204}\text{Pb}$ – $^{208}\text{Pb}/^{204}\text{Pb}$ in primitive Turkana Tertiary and Quaternary basalts show significant overlap, although Tertiary lavas extend towards HIMU-dominated St. Helena basalts. (e) Regional $^{143}\text{Nd}/^{144}\text{Nd}$ – $^{206}\text{Pb}/^{204}\text{Pb}$ variations indicate mixing among high- μ , lithospheric and Afar plume source components. (f) Jarigole basalts and picrites have Pb–Sr isotopic compositions that plot within the field of HIMU lavas (Stracke *et al.*, 2005). Tie-lines connect samples that were analyzed by both TIMS and higher precision MC-ICP-MS methods following leaching of 2–5 mm chips. It should be noted that the more precise data consistently displace the analyses towards the field of HIMU.

from moderately radiogenic values (at Mt. Kulal) to much lower values (at Longipi) that overlap those for modern mafic lavas of the Afar plume from Djibouti (Deniel *et al.*, 1994; Fig. 6). Tertiary Turkana mafic lavas show greater scatter in $^{207}\text{Pb}/^{204}\text{Pb}$ values than is observed in the Quaternary suite or basalts from MORB suites such as the West Sheba Ridge (Schilling *et al.*, 1998), although the Jarigole picrites again define a consistent narrow compositional range.

Helium isotopic data obtained on three Jarigole picrites fall within analytical error (6.2–6.6 R_A , where R_A indicates the ratio of $^3\text{He}/^4\text{He}$ measured in the sample to that of the atmosphere); these values are significantly lower than data obtained on Oligocene to Recent basalts from central Ethiopia (up to 19 R_A ; Marty *et al.*, 1993, 1996; Scarsi & Craig, 1996) and are consistent with sites of HIMU volcanism (e.g. Graham *et al.*, 1992; Barfod *et al.*, 1999; Hilton *et al.*, 2000).

DISCUSSION

Source regions and melting history in the Turkana Rift

Lithospheric assimilation

Most samples within the Turkana suite have geochemical signatures that are inconsistent with significant contamination by crustal or mantle lithospheric melts. One Pliocene lava (KL 18) has the most enriched $^{87}\text{Sr}/^{86}\text{Sr}$ and ϵ_{Nd} values (0.7047 and 0.7, respectively) observed at Turkana, as well as high Ba/Nb (18.3) and Ba/Th (217), suggesting a contribution from either the crust or the lithospheric mantle. It is noteworthy for the discussion that follows that this sample does not have the most radiogenic $^{206}\text{Pb}/^{204}\text{Pb}$ of the suite, but does have the most radiogenic $^{207}\text{Pb}/^{204}\text{Pb}$ at the edge of the resolution by the TIMS technique. A second Pliocene sample (LGP 4) with similar Ba enrichment has a radiogenic Sr isotopic signature (0.7042) that is accompanied by more depleted values of ϵ_{Nd} (5.0), $^{206}\text{Pb}/^{204}\text{Pb}$ and $^{207}\text{Pb}/^{204}\text{Pb}$, suggesting either a sublithospheric source or a different lithospheric component. These features are also observed in two Quaternary Turkana lavas, interpreted as lithospheric mantle melts (Furman *et al.*, 2004), but are absent among samples older than ~3.5 Ma. The isotopic signatures of these samples are similar to the radiogenic end of the Red Sea array (Schilling *et al.* 1998), but their trace element compositions suggest a lithospheric origin.

Minor variations in chemical parameters sensitive to crustal contamination also exist among mafic lavas with $^{87}\text{Sr}/^{86}\text{Sr}$ values <0.7035 (e.g. K_2O , Ba/Th, Ce/Pb, particularly among Group A Kajong lavas), but the magnitude of these variations is small and could, in some cases, result from pressure-dependent partitioning

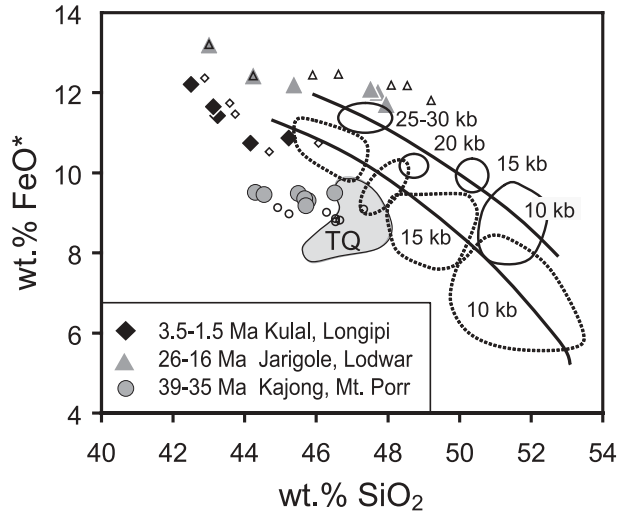


Fig. 7. FeO^* vs SiO_2 for selected EARS mafic suites and experimental melts in equilibrium with mantle peridotite (Baker & Stolper, 1994; Kushiro, 1996). Dotted lines encircle fields for experimental melts coexisting with cpx + oliv + opx; continuous lines enclose fields for liquids coexisting with oliv + opx after higher degrees of melting. Major element compositions were renormalized with total iron as FeO , then corrected for olivine fractionation to correspond to experimentally derived melts of fertile peridotite (Mg-number ~72); only samples with Mg-number >62 were corrected using this procedure. Smaller symbols indicate the original data for comparison. Tertiary Turkana basalts define three groups: (1) Kajong and Mt. Porr lavas indicate derivation at pressures ~20 kbar, similar to depths inferred for melting along the Main Ethiopian Rift and in Erta' Ale (Barrat *et al.*, 1998; Hart *et al.*, 1989; Furman *et al.*, 2006). (2) Jarigole and Lodwar picrites and basalts record pressures of 25–30 kbar. These samples have unusually high FeO^* contents consistent with high extents of melting. (3) Basalts from Mt. Kulal and Longipi also indicate melting pressures of 25–30 kbar, but at substantially lower FeO^* values. Quaternary basalts from Turkana (Furman *et al.*, 2004) and the Red Sea (Volker *et al.*, 1997) indicate the lowest melting pressures. Pressures and degrees of melting estimated on the basis of this diagram are approximate.

behavior of these elements during progressive melting of a pyroxene-bearing source (Blundy *et al.*, 1998). We emphasize that the majority of Turkana samples are MgO-rich with incompatible trace element abundances within the range of mantle-derived melts, making it unlikely that they have experienced substantial crustal assimilation. In assessing the mineralogy and thermal structure of the Turkana source regions we focus on mafic lavas that display the least evidence for interaction with crustal and mantle lithospheric melts.

Depth and extent of melting

Isotopic and trace element considerations indicate that all Turkana mafic lavas are derived from a source region that is enriched relative to the depleted mantle, and for this reason we compare them with experimental melts of fertile peridotite. The SiO_2 and FeO^* contents of primitive Turkana lavas (back-corrected for olivine fractionation; Fig. 7) plot near the range of experimentally

derived melts of fertile peridotite at pressures of ~ 20 – 30 kbar (Baker & Stolper, 1994; Kushiro, 1996). This result corresponds well with inferences based on the Tb/Yb_n values (Fig. 5) of Tertiary Turkana lavas that indicate a depth of melting at or above the garnet–spinel transition (~ 80 km depth, or ~ 25 kbar). There is a strong temporal pattern to the inferred depths of melting. The oldest samples (Kajong and Mt. Porr, 35–39 Ma) record the lowest apparent pressures of melting, whereas Plio-Pleistocene lavas (Longipi) and ~ 20 – 23 Ma basalts and picrites (Lodwar and Jarigole) plot at substantially higher pressures.

The low FeO^* and SiO_2 contents of most Turkana mafic lavas (relative to the experimental fields; Fig. 7) suggest melting in the presence of residual clinopyroxene. The Jarigole and Lodwar picrites have higher FeO^* and SiO_2 contents, suggesting higher degrees of melting ($\sim 15\%$ for fertile peridotite, see Kushiro, 1996). It should be noted, however, that there is no evidence to suggest that the source region for the Turkana mafic lavas is either clinopyroxenitic or olivine-free (e.g. Sobolev *et al.*, 2005). Lavas derived from pyroxenite are expected to have unusually high contents of Na_2O and SiO_2 (Hirschmann, 2000; Pickering-Witter & Johnston, 2000; le Roux *et al.*, 2002) that are not observed in this sample suite.

Sub-lithospheric mantle contributions

Sr–Nd–Pb isotopic compositions of the Tertiary Turkana mafic lavas require material inputs from one or more sub-lithospheric sources. A similar conclusion was reached by Furman *et al.* (2004) with regard to the Quaternary Turkana basalts, and this study extends that interpretation back in time to the onset of regional extension and volcanism. Tertiary lavas define a wider range in radiogenic lithophile isotopic compositions than the Quaternary suite, although the two groups overlap substantially; all Plio-Pleistocene lavas plot within fields defined by the Quaternary basalts (Fig. 6).

The voluminous second phase of Turkana volcanism, represented here by ~ 20 Ma basalts and picrites from Jarigole and Lodwar, has a restricted range of Sr–Nd–Pb–He isotopic values that require a high- μ mantle source. This composition apparently represents an end-member that contributes to Turkana magmatism—as well as that of southern Ethiopia—throughout the regional ~ 40 Myr volcanic history. Turkana samples that are clearly not affected by crustal or lithospheric processes define mixing trends between the proposed common source composition for global magmatism—FOZO (Hart *et al.*, 1992) or C (Hanan & Graham, 1996)—and this high- μ end-member (Fig. 6).

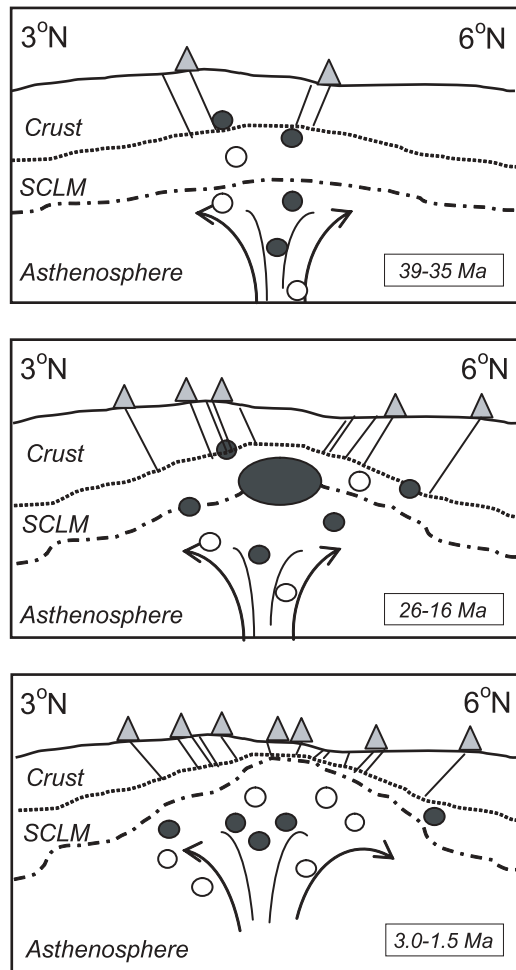


Fig. 8. Schematic illustration of the linked evolution of Turkana rifting and magmatism (see text for discussion). The different shades of ascending material indicate chemical heterogeneity within the inferred plume; dark blobs represent source material of high- μ isotopic character that are present throughout the history of Turkana magmatism but are dominant for a brief episode at ~ 20 Ma.

Geodynamic evolution of the Turkana region

Rifting and volcanism

The Turkana Rift occupies a significant position within the overall architecture of the East African Rift System. It preserves evidence for the earliest phases of both magmatism and extension along the entire rift, and marks the transitional junction between the north–south-trending Kenya Rift and the NE–SW-trending Main Ethiopian Rift. Understanding the evolution of mantle source regions during progressive lithospheric thinning and/or removal therefore provides insight into the overall mechanisms of continental extension. We interpret the Turkana data in terms of plume–lithosphere interaction during rifting as shown schematically in Fig. 8 and described below.

Relationships between FeO* and SiO₂ indicate that the oldest (39–35 Ma) basanite lavas from Kajong and Mt. Porr were derived at pressures of 15–20 kbar (Fig. 7), corresponding to depths of 50–65 km. A few of these early lavas record interaction with continental crust or mantle lithosphere, presumably during ascent through a thick, cool section (Fig. 8). The Sr–Pb isotopic composition of the primitive basanites includes a high- μ component that is, however, clearly unrelated to crustal and/or mantle lithospheric contamination; this component is not observed in contemporaneous lavas from southern Ethiopia (Stewart & Rogers, 1996), which are derived largely from the mantle lithosphere. The 39–35 Ma episode of Turkana mafic volcanism precedes faulting and regional uplift, suggesting that it does not reflect adiabatic decompression melting as a passive response to lithospheric stretching, but rather requires substantial heat input, probably from a mantle plume (e.g. Ebinger *et al.*, 2000).

Primitive Jarigole and Lodwar basalts and picrites provide strong evidence for a thermal and chemical anomaly (i.e. plume) beneath the Turkana area at ~20 Ma (Fig. 8). Jarigole and Lodwar mafic lavas appear to be derived by the greatest degree of melting recorded in the Turkana suite, and their inferred depth of origin is ~85–100 km (Fig. 7); these observations suggest a significant thermal event that is constrained in both space and time, such as a pulse in plume activity. The ~20 Ma phase of activity is associated with both northward and southward propagation of rifting and volcanism, as indicated by progressively younger ages of fault-bounded rift basins and basalts in southern Ethiopia away from Turkana, as well as to the south along the Kenya Rift (George *et al.*, 1998; Ebinger *et al.*, 2000). Rift basins in southern Ethiopian that developed at 18–10 Ma (e.g. Getra-Kele, Chew Bahir, Chamo; Fig. 1) are oriented north–south, like those in Turkana and Kenya, rather than NE–SW as in the Main Ethiopian Rift, where they are probably related to Red Sea rifting (e.g. Ebinger *et al.*, 2000). Miocene faults, basins and volcanic rocks in the Kenya and Western Rifts also young consistently away from Turkana, supporting our interpretation that a major pulse of magmatic activity triggered rift propagation.

The distinctive Sr–Nd–Pb–He isotopic signatures of the Jarigole picrites approach those of the HIMU mantle end-member (e.g. Chaffey *et al.*, 1989; Graham *et al.*, 1992; Stracke *et al.*, 2005). The incompatible trace element ratios of these lavas fall consistently within the range of HIMU basalts and other mantle-derived melts, and show no evidence of contamination by crustal materials. The lack of crustal overprint probably results from the greater volume of lava erupted during this period relative to that of the 39–35 Ma episode, as well as the progressive maturation of transport pathways through the lithosphere. The isotopic signatures of 19–11 Ma southern

Ethiopian basalts appear to show mixing between the high- μ component and a source area with more enriched Sr–Nd isotopic characteristics (Fig. 6), which could be the Afar mantle plume, the Ethiopian lithosphere, or a combination of the two. It is worth noting that the southern Ethiopian lavas do not include primitive lavas with >8.7 wt % MgO. Although many of them have ²⁰⁶Pb/²⁰⁴Pb values characteristic of high- μ volcanism, a subset also show the high ²⁰⁷Pb/²⁰⁴Pb values indicative of crustal involvement (Fig. 6).

Plio-Pleistocene to Recent Turkana mafic lavas show the effects of a shift from localized volcanism to a more distributed and laterally extensive array of rift structures. During this period the locus of extension moved eastward, with development of the Ririba Volcanic Zone and related north–south-trending features in southern Ethiopia (e.g. Hendrie *et al.*, 1994; Ebinger *et al.*, 2000) although the rift axis beneath Lake Turkana remained a zone of active faulting and magmatism (Dunkleman *et al.*, 1988). Latest Tertiary Turkana lavas from Longipi (east of Lake Turkana; Fig. 1) record melting at pressures of ~20–30 kbar (Fig. 7), whereas Quaternary lavas from neighboring South Island formed at 15–20 kbar, consistent with the extremely thin crustal section observed seismically (~20 km; Simiyu & Keller, 1997, and references therein). Some of the ≤3.5 Ma Turkana lavas record melting of amphibole-bearing peridotite, presumably within the lithospheric mantle. The youngest southern Ethiopian lavas also show both lithospheric and sub-lithospheric contributions as indicated by extremely heterogeneous Sr–Nd isotopic signatures (Fig. 6). The short spatial scale over which melting and eruptive processes sample both lithospheric and sub-lithospheric source materials (<1 km at Bird Nest Island; Furman *et al.*, 2004) suggests that magmas ascend along the locally rough topography of the lithosphere–asthenosphere boundary (Fig. 8).

Occurrence of high- μ volcanism in East Africa

Mafic lavas erupted in many parts of Africa and the Near East since 100 Ma display radiogenic isotope signatures that indicate contributions from high- μ component(s) (Fig. 9 and references therein). Some of these suites are alkalic, and most have isotopic compositions that do not overlap those of the Turkana picrites (²⁰⁶Pb/²⁰⁴Pb ~20.5 and ⁸⁷Sr/⁸⁶Sr ~0.703). Among both recent and pre-Miocene volcanic rocks in the African Rift there is a broad increase in ²⁰⁶Pb/²⁰⁴Pb values with increasing distance from the center of the inferred modern Afar plume as one moves southward towards Turkana (Fig. 9). Oligocene flood basalts associated with plume head impact beneath Ethiopia and Yemen apparently lack this compositional component, as they have

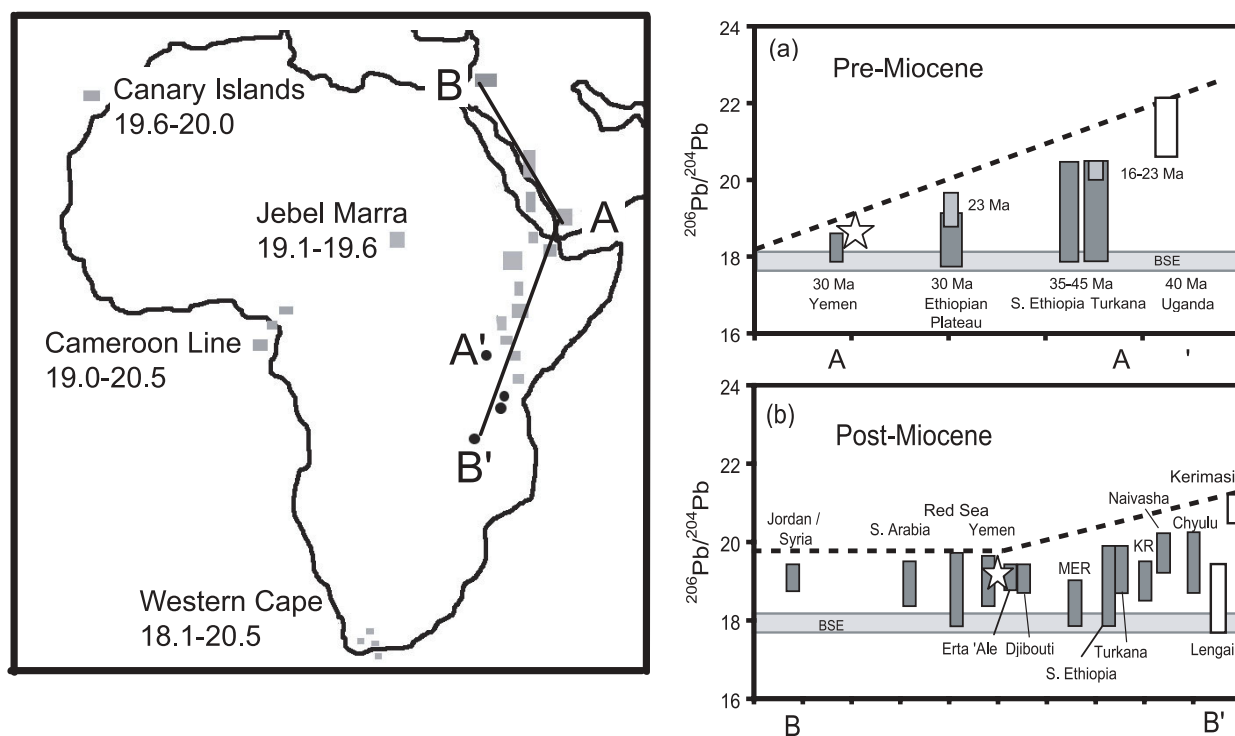


Fig. 9. Variation in $^{206}\text{Pb}/^{204}\text{Pb}$ as a function of distance from the Afar region. The map indicates areas from which data were used to construct the graphs; only samples with >6 wt % MgO and $^{87}\text{Sr}/^{86}\text{Sr}$ isotope values <0.7040 are plotted. Grey squares indicate mafic silicate lavas; ●, carbonatites. Pb isotope values ($^{206}\text{Pb}/^{204}\text{Pb}$) for Jebel Marra, the Cameroon Line, Canary Islands and South Africa are shown for comparison and are not plotted. Distance to Afar is calculated by projecting each locality onto the black lines. Pb isotope compositions observed along the EARS south of Afar fall within a triangular envelope defined by Bulk Silicate Earth (BSE), the modern Afar plume (open star), and East African carbonatites (white rectangles). This relationship is not observed among samples from the Arabian Shield and Red Sea. (See text for a full discussion.) Sources of data: Davies & Macdonald, 1987; Halliday *et al.*, 1988, 1990; Davidson & Wilson, 1989; Hart *et al.*, 1989; Chazot & Bertrand, 1993; Deniel *et al.*, 1994; Simonetti & Bell, 1995; Bell & Simonetti, 1996; Stewart & Rogers, 1996; Kalt *et al.*, 1997; Volker *et al.*, 1997; Barrat *et al.*, 1998; George *et al.*, 1998; Pik *et al.*, 1999; Hilton *et al.*, 2000; Rogers *et al.*, 2000; Bell & Tilton, 2001; Macdonald *et al.*, 2001; Späth *et al.*, 2001; Janney *et al.*, 2002; Bertrand *et al.*, 2003; Shaw *et al.*, 2003; Furman *et al.*, 2004, 2006; Kieffer *et al.*, 2004.

$^{206}\text{Pb}/^{204}\text{Pb} \leq 19.0$ (Pik *et al.*, 1999; Kieffer *et al.*, 2004). In contrast, Eocene to Oligocene mafic lavas from Turkana (this study) and southern Ethiopia (Stewart & Rogers, 1996) as well as carbonatites from several localities in eastern Uganda (Bell & Tilton, 2001) extend to higher $^{206}\text{Pb}/^{204}\text{Pb}$ values that are more readily associated with high- μ source contributions (Fig. 9). Farther south, olivine melilitites and alkali basalts erupted at 58–76 Ma in the Western Cape region also include high- μ compositions (Janney *et al.*, 2002). The He isotopic database for this region is more limited, but where data are available they indicate high $^3\text{He}/^4\text{He}$ values associated with the Afar plume (up to $19 R_A$; Marty *et al.*, 1996; Scarsi & Craig, 1996) and lower values more typical of high- μ basalts along the Cameroon Line (Barfod *et al.*, 1999; Aka *et al.*, 2004) and at Turkana.

The origin of the high- μ signature in African volcanic rocks and the broader geochemical systematics of high- μ ocean island rocks remain topics of debate. Recently, Stracke *et al.* (2005) suggested that this component represents recycled ocean crust or carbonate that is

samplled within a mantle plume (e.g. Graham *et al.*, 1992; Bell & Tilton, 2001; Hoernle *et al.* 2002). Janney *et al.* (2002) proposed that the high- μ signature associated with post-Cretaceous alkaline rocks throughout Africa arises from sublithospheric melting of pods of recycled oceanic material that are mobilized by a large regional mantle upwelling, perhaps the South African superplume. On the other hand, widespread volcanic rocks with high- μ tendencies ($^{206}\text{Pb}/^{204}\text{Pb} = 18.6$ – 19.5) in the Arabian Plate and the Red Sea region are interpreted as melts of the lithospheric mantle (Bertrand *et al.*, 2003; Shaw *et al.*, 2003).

The isotopic signatures of the Jarigole picrites are a testament to the influence of a high- μ source in Turkana in the Tertiary: the $^{206}\text{Pb}/^{204}\text{Pb}$ values (averaging 20.3 in the picrites) fall on the border of the new HIMU classification proposed by Stracke *et al.* (2005). These radiogenic Pb isotopic signatures are associated with depleted $^{87}\text{Sr}/^{86}\text{Sr}$ values (averaging <0.7032) and HIMU-like $^3\text{He}/^4\text{He}$ signatures ($\sim 6 R_A$). The four Turkana samples with high- μ isotopic characteristics

have narrow ranges in diagnostic incompatible trace element ratios (e.g. Nb/U, Ce/Pb, Ba/Nb, Ba/Th, Ba/Rb) that overlap those of St. Helena HIMU lavas (Chaffey *et al.*, 1989), whereas the remaining Turkana samples and proposed high- μ lavas from the Arabian Shield (Bertrand *et al.*, 2003) have much more variable isotopic and incompatible trace element ratios that are consistent with contributions from the mantle lithosphere.

Several lines of evidence indicate that the high- μ source component does not reside within the lithospheric mantle beneath Turkana. First, the inferred depth of melting (~ 85 – 100 km) is below the base of the continental lithospheric mantle at ~ 20 Ma, as deduced from seismic information and structural basin analysis (Morley *et al.*, 1992; Hendrie *et al.*, 1994). Second, although melting of eclogite detached from the subcontinental lithospheric mantle in the Turkana region during rifting could produce the observed picritic melts, the time scales typically inferred for this process (30–75 Myr; Anderson, 2005) are substantively longer than the offset between the initiation of extension and the occurrence of high- μ magmatism in Turkana. Finally, the high- μ influence in Turkana is observed most clearly in basalts and picrites from a discrete pulse of volcanic activity (~ 20 – 23 Ma) associated with the onset of northward and southward propagation of the Main Ethiopian and Kenya Rifts. This short-lived voluminous magmatic pulse and the moderate to large extents of melting inferred on the basis of major element compositions (Fig. 7) require an anomalously warm environment, in keeping with the expected melting regime within a mantle plume. In this regard, the Turkana high- μ lavas differ significantly from the small-volume high- μ melilitites from the Western Cape, South Africa (Janney *et al.*, 2002).

Collectively, the high- μ lavas record the highest degrees of melting at the greatest pressures (~ 25 – 30 kbar) observed over a 40 Myr period of volcanism in Turkana. The existence of the high- μ signature in Turkana, in products with trace and major element signatures indicative of high degrees of polybaric melting originating at high pressures, is best reconciled with melting of exotic source materials in the asthenosphere. The spatial and temporal distribution of lavas with high- μ isotopic characteristics indicates that this geochemical component is not associated with the Afar plume head (Fig. 9). As outlined below, the occurrence of the high- μ influence across and throughout Africa is consistent with an association with the upwelling South African superplume (see Janney *et al.*, 2002).

Sublithospheric structure beneath the East African Rift System

Early two-plume models (George *et al.* 1998; Rogers *et al.* 2000) were based on the Sr–Nd isotopic compositions of

lavas from southern Ethiopia and the Kenya Rift. The current study, which incorporates Sr–Nd–Pb–He isotopic observations over a much larger region and time frame, requires long-lived, isolated and geochemically distinct source domains to produce the diverse range of magmas originating from beneath the African lithosphere. Specifically, we need to explain the contemporaneous occurrence of high- μ (relatively high $^{206}\text{Pb}/^{204}\text{Pb}$, low $^{87}\text{Sr}/^{86}\text{Sr}$ and low- ^3He) volcanism at Turkana and rather lower $^{206}\text{Pb}/^{204}\text{Pb}$, high- ^3He magmatism in Afar. The question remains whether two geochemically distinct plumes are required to explain the regional geochemical and geophysical observations.

The geochemical variations alone do not require two distinct plumes, but could reflect heterogeneity within one plume. This suggestion follows from a single-plume model proposed by Ebinger & Sleep (1998) attributing Cenozoic African Rift volcanism to plume head impact beneath southern Ethiopia at ~ 45 Ma, with lateral transport of plume material along zones of thinned lithosphere. The spatial proximity of lavas with this degree of Pb and He isotopic variability is not unique to East Africa, as it is also observed in the southern Pacific, where basalts from Samoa, Pitcairn and some of the Society Islands (high- ^3He), and those from the Cook–Austral islands (HIMU-affinity), are all associated with the South Pacific Superplume (e.g. Farley *et al.*, 1992; Hanyu *et al.*, 1999; Courtillot *et al.*, 2003; Lassiter *et al.*, 2003).

The geophysical evidence, however, may require two separate upper-mantle structures. There is a growing body of seismic information indicating plume stems beneath Afar and Tanzania that are linked to lower mantle features. Beneath Afar, S-wave tomographic imaging shows a thermal anomaly that reaches ~ 500 km below the surface (Debayle *et al.*, 2001; Benoit *et al.*, 2003). Montelli *et al.* (2004) suggested that this feature extends to depths approaching 1200 km, well below the Transition Zone, hence requiring a deep mantle origin. Beneath the Tanzania craton, Nyblade *et al.* (2000) and Weeraratne *et al.* (2003) documented an upper mantle thermal anomaly that is too large to be sustained by flow of plume material along the rift axis, and is interpreted as an ascending plume head. The continuation of this structure as a plume tail at depth is unclear, as is its possible connection to the South African superplume. The geophysical evidence thus supports two distinct upper- to mid-mantle thermal anomalies, or plumes. The depth of origin of these two features is unclear, as they may merge below 1000 km as seen with other plume pairs (Azores and Canaries, Ascension and St. Helena; Montelli *et al.*, 2004). In this case, both thermal anomalies may be derived from the South African superplume, a well-documented (Ritsema *et al.*, 1999; Gurnis *et al.*, 2000; Zhao, 2001; Ni *et al.*, 2002)

feature of the deep mantle. Current tomographic models are unable to resolve the fine structure of the mid-mantle, leaving open the question of whether this feature reaches the shallow mantle beneath the African Rift.

The observations presented here can be reconciled through a modified one-plume model that allows for multiple plume stems arising from a common large plume at depth (Ishida *et al.* 1999; Davaille *et al.* 2003; Farnetani & Samuel, 2003). The plume stems supporting volcanism in Turkana and in the Afar are proposed to contain lenses of isotopically distinct materials, and hence record large-scale heterogeneity within the South African superplume. This result is consistent with numerical simulations of plume geochemical structures (Samuel & Farnetani, 2003), which demonstrate that large geochemical and isotopic contrasts can exist over time and length scales consistent with those observed in eastern Africa. These simulations show that chemically distinct components present in the lower mantle can ascend through the mantle without full-scale mixing, and suggest that chemical heterogeneities in the lower mantle may in fact lead to a complex range in plume shapes and sizes.

SUMMARY

Primitive mafic lavas of Tertiary age from Turkana, Kenya, provide insight into the magmatic processes associated with the earliest phase of continental extension in the central East African Rift. Alkalic and tholeiitic basalt lavas from Turkana display a wide range in incompatible trace element abundances and Sr–Nd–Pb isotope ratios that are probably the result of variations in both source composition and melting conditions as a function of time. The oldest basanite lavas (up to 40 Ma) show evidence of crustal contamination resulting from interaction along immature magmatic pathways in the early evolution of the rift. A significant volume of primitive basalts and picrites with high- μ Sr–Nd–Pb–He isotopic signatures was erupted for a restricted period of time from 23 to 20 Ma. This eruptive episode is associated with rift propagation both to the north and south, suggesting that it is tectonically significant to the overall evolution of the African Rift. Mafic lavas from this period were derived by the greatest extents of melting recorded at Turkana and at the greatest pressures (>25 kbar). Late Tertiary Turkana lavas, like the Quaternary Turkana suite (Furman *et al.*, 2004), show local involvement of continental mantle lithosphere that suggests the rapid development of steep topography across the lithosphere–asthenosphere boundary associated with the interaction of the Main Ethiopian and Kenya rifts.

The high- μ isotopic signature observed in the Jarigole mafic lavas is not derived from the *in situ* mantle

lithosphere, but rather requires a sub-lithospheric origin. These isotopic features are not observed in lavas of any age erupted in the Afar region, and are interpreted as evidence for a long-lived mantle plume that is spatially, temporally and geochemically heterogeneous. We suggest that the high- μ component—presumably a pod of recycled ancient oceanic crust—was entrained by upwelling plume material, rises passively at the same time as the plume, or forms an integral part of the upwelling plume itself. We attribute this heterogeneity to the South African superplume, where large-scale internal variations in source composition are manifest in a wide range of eruptive isotopic signatures across Africa.

ACKNOWLEDGEMENTS

This paper grew out of the M.S. thesis of K.M.K., who gratefully acknowledges fellowship support from the Department of Geosciences at Penn State. We are very grateful for He isotope analyses performed by D. Graham, and for Ar dates obtained by R. Duncan. Major and trace element analyses at Duke University were performed by M. Rudnicki and G. Dwyer, and we thank E. Klein for making her facility available to us. We thank Haibo Zou for conducting the TIMS analyses. T.F. supported this work through NSF EAR-0207764 and a George H. Deike, Jr grant from the College of Earth and Mineral Sciences at Penn State. J.G.B. is appreciative of support during the preparation of this manuscript from NSF EAR-0338385, as well as funds from the UNH College of Engineering and Physical Sciences. Thoughtful comments from S. Gibson, J. Mahoney and D. Geist have served to clarify our thinking and improve the manuscript.

REFERENCES

- Aka, F. T., Nagao, K., Kusakabe, M., Sumino, H., Tanyileke, G., Ateba, B. & Hell, J. (2004). Symmetrical helium isotope distribution on the Cameroon Volcanic Line, West Africa. *Chemical Geology* **203**, 205–223.
- Albarède, F., Télouk, P., Blichert-Toft, J., Boyet, M., Agraniér, A. & Nelson, B. (2004). Precise and accurate isotopic measurements using multiple-collector ICPMS. *Geochimica et Cosmochimica Acta* **68**, 2725–2744.
- Anderson, D. (2005). Large igneous provinces, delamination, and fertile mantle. *Elements* **1**, 271–275.
- Baker, M. B. & Stolper, E. M. (1994). Determining the composition of high-pressure mantle melts using diamond aggregates. *Geochimica et Cosmochimica Acta* **58**, 2811–2827.
- Barfod, D. N., Ballentine, C. J., Halliday, A. N. & Fitton, J. G. (1999). Noble gases in the Cameroon line and the Ne, Ne, and Ar isotopic compositions of high μ (HIMU) mantle. *Journal of Geophysical Research* **104**, 29509–29527.
- Barrat, J. A., Fourcade, S., Jahn, B. M., Cheminée, J. L. & Capdevila, R. (1998). Isotope (Sr, Nd, Pb, O) and trace element

- geochemistry of volcanics from the Erta' Ale range (Ethiopia). *Journal of Volcanology and Geothermal Research* **80**, 85–100.
- Bell, K. & Simonetti, A. (1996). Carbonatite magmatism and plume activity: implications from the Nd, Pb and Sr isotope systematics of Oldoinyo Lengai. *Journal of Petrology* **37**, 1321–1339.
- Bell, K. & Tilton, G. R. (2001). Nd, Pb and Sr isotopic compositions of East African carbonatites; evidence for mantle mixing and plume inhomogeneity. *Journal of Petrology* **42**, 1927–1945.
- Benoit, M., Nyblade, A., Tuji, M., Ayele, A., Asfaw, L., Langston, C. & VanDecar, J. (2003). Upper mantle seismic velocity structure beneath East Africa and the depth extent of thermal anomalies. *Geophysical Research Abstracts* **5**, number 07361.
- Bertrand, H., Chazot, G., Blichert-Toft, J. & Thoral, S. (2003). Implications of widespread high- μ volcanism on the Arabian Plate for Afar mantle plume and lithosphere composition. *Chemical Geology* **198**, 47–61.
- Bloomer, S. H., Curtis, P. C. & Karson, J. A. (1989). Geochemical variation of Quaternary basaltic volcanics in the Turkana Rift, northern Kenya. *Journal of African Earth Science* **8**, 511–532.
- Blundy, J. D., Robinson, J. A. C. & Wood, B. (1998). Heavy REE are compatible in clinopyroxene on the spinel lherzolite solidus. *Earth and Planetary Science Letters* **160**, 493–504.
- Boynnton, W. V. (1984). Cosmochemistry of the rare earth elements: meteorite studies. In: Henderson, P. (ed.) *Rare Earth Element Geochemistry*. Amsterdam: Elsevier, pp. 63–114.
- Brotzu, P., Morbidelli, L., Nicoletti, M., Piccirillo, E. M. & Traversa, G. (1984). Miocene to Quaternary volcanism in eastern Kenya; sequence and geochronology. *Tectonophysics* **101**, 75–86.
- Chaffey, D. J., Cliff, R. A. & Wilson, B. M. (1989). Characterization of the St. Helena magma source. In: Saunders, A. D. & Norry, M. J. (eds) *Magmatism in the Ocean Basins*. Geological Society, London, *Special Publications* **42**, 257–276.
- Chazot, G. & Bertrand, H. (1993). Mantle sources and magma–continental crust interactions during early Red Sea–Gulf of Aden rifting in Southern Yemen; elemental and Sr, Nd, Pb isotope evidence. *Journal of Geophysical Research* **98**, 1819–1835.
- Courtillot, V., Davaille, A., Besse, J. & Stock, J. (2003). Three distinct types of hotspots in the Earth's mantle. *Earth and Planetary Science Letters* **205**, 295–308.
- Davaille, A., Le Bars, M. & Carbonne, C. (2003). Thermal convection in a heterogeneous mantle. *Comptes Rendus de l'Académie des Sciences, Géoscience* **335**, 141–156.
- Davidson, J. P. & Wilson, I. R. (1989). Evolution of an alkali basalt–trachyte suite from Jebel Marra volcano, Sudan, through assimilation and fractional crystallization. *Earth and Planetary Science Letters* **95**, 141–160.
- Davies, G. R. & Macdonald, R. (1987). Crustal influences in the petrogenesis of the Naivasha basalt–comendite complex: combined trace element and Sr–Nd–Pb isotope constraints. *Journal of Petrology* **28**, 1009–1031.
- Debayle, E., Leveque, J.-J. & Cara, M. (2001). Seismic evidence for a deeply rooted low-velocity anomaly in the upper mantle beneath the northeastern Afro/Arabian continent. *Earth and Planetary Science Letters* **193**, 423–436.
- Deniel, C., Vidal, P., Coulon, C., Vellutini, P.-J. & Pigué, P. (1994). Temporal evolution of mantle sources during continental rifting: the volcanism of Djibouti. *Journal of Geophysical Research* **99**, 2853–2869.
- Dunkleman, T. J., Karson, J. A. & Rosendahl, B. R. (1988). Structural style of the Turkana Rift. *Geology* **16**, 258–261.
- Ebinger, C. J. & Ibrahim, N. H. (1994). Multiple episodes of rifting in Central and East Africa; a re-evaluation of gravity data. *Geologische Rundschau* **83**, 689–702.
- Ebinger, C. J. & Sleep, N. H. (1998). Cenozoic magmatism throughout east Africa resulting from impact of a single plume. *Nature* **395**, 788–791.
- Ebinger, C. J., Yemane, T., Harding, D. J., Tesfaye, S., Kelley, S. & Rex, D. C. (2000). Rift deflection, migration, and propagation: linkage of the Ethiopian and Eastern rifts, Africa. *Geological Society of America Bulletin* **112**, 163–176.
- Farley, K. A., Natland, J. H. & Craig, H. (1992). Binary mixing of enriched and undegassed (primitive?) mantle components (He, Sr, Nd, Pb) in Samoan lavas. *Earth and Planetary Science Letters* **111**, 183–199.
- Farnetani, C. & Samuel, H. (2003). Lagrangian structures and stirring in the Earth's mantle. *Earth and Planetary Science Letters* **206**, 335–348.
- Furman, T., Bryce, J. G., Karson, J. & Iotti, A. (2004). East African Rift System (EARS) plume structure: insights from Quaternary mafic lavas of Turkana, Kenya. *Journal of Petrology* **45**, 1069–1088.
- Furman, T., Bryce, J., Rooney, T., Yirgu, G. & Ayalew, D. (2006). Heads and tails: 30 million years of the Afar plume. In: Yirgu, G., Ebinger, C. J. & Maguire, P. K. H. (eds) *The Structure and Evolution of the East African Rift System in the Afar Volcanic Province*. Geological Society, London, *Special Publications* **259**, 97–121.
- George, R. & Rogers, N. (2002). Plume dynamics beneath the African plate inferred from the geochemistry of the Tertiary basalts of southern Ethiopia. *Contributions to Mineralogy and Petrology* **144**, 286–304.
- George, R., Rogers, N. & Kelley, S. (1998). Earliest magmatism in Ethiopia: evidence for two mantle plumes in one flood basalt province. *Geology* **26**, 923–926.
- Graham, D. W., Humphris, S. E., Jenkins, W. J. & Kurz, M. D. (1992). Helium isotope geochemistry of some volcanic rocks from Saint Helena. *Earth and Planetary Science Letters* **110**, 121–131.
- Graham, D. W., Larsen, L. A., Hanan, B. B., Storey, M., Pedersen, A. K. & Lupton, J. E. (1998). Helium isotope composition of the early Iceland mantle plume inferred from the Tertiary picrites of West Greenland. *Earth and Planetary Science Letters* **160**, 241–255.
- Gurnis, M., Mitrovica, J. X., Ritsema, J. & van Heijst, H.-J. (2000). Constraining mantle density structure using geological evidence of surface uplift rates: the case of the African Superplume. *Geochemistry Geophysics Geosystems* **2**, Paper number 1999GC000035.
- Halliday, A. N., Dicken, A. P., Fallick, A. E. & Fitton, J. G. (1988). Mantle dynamics: a Nd, Sr, Pb and O isotope study of the Cameroon Line volcanic chain. *Journal of Petrology* **29**, 181–211.
- Halliday, A. N., Davidson, J. P., Holden, P., DeWolf, C., Lee, D.-C. & Fitton, J. G. (1990). Trace-element fractionation in plumes and the origin of HIMU mantle beneath the Cameroon line. *Nature* **347**, 523–528.
- Hanan, B. B. & Graham, D. W. (1996). Lead and helium isotope evidence from oceanic basalts for a common deep source of mantle plumes. *Science* **272**, 991–995.
- Hanyu, T., Kaneoka, I. & Nagao, K. (1999). Noble gas study of HIMU and EM ocean island basalts in the Polynesian region. *Geochimica et Cosmochimica Acta* **63**, 1181–1201.
- Hart, S. R., Hauri, E. H., Oschmann, L. A. & Whitehead, J. A. (1992). Mantle plumes and entrainment: isotopic evidence. *Science* **256**, 517–520.
- Hart, W. K., WoldeGabriel, G., Walter, R. C. & Mertzman, S. A. (1989). Basaltic volcanism in Ethiopia: constraints on continental rifting and mantle interactions. *Journal of Geophysical Research* **94**, 7731–7748.
- Hendrie, D. B., Kuszniir, N. J., Morley, C. K. & Ebinger, C. J. (1994). Cenozoic extension in northern Kenya: a quantitative model of rift basin development in the Turkana region. *Tectonophysics* **236**, 409–438.

- Hilton, D. R., Macpherson, C. G. & Elliott, T. R. (2000) Helium isotope ratios in mafic phenocrysts and geothermal fields from La Palma, the Canary Islands (Spain); implications for HIMU mantle sources. *Geochimica et Cosmochimica Acta* **64**, 2119–2132.
- Hirschmann, M. M. (2000). Mantle solidus; experimental constraints and the effects of peridotite composition. *Geochemistry, Geophysics, Geosystems* **1**, paper number 2000GC000070, 24.
- Hoernle, K., Tilton, G., Le Bas, M. J., Duggen, S. & Garbe-Schonberg, D. (2002). Geochemistry of oceanic carbonatites compared with continental carbonatites: mantle recycling of oceanic crustal carbonate. *Contributions to Mineralogy and Petrology* **142**, 520–542.
- Ishida, M., Maruyama, S., Suetsugu, D., Matsuzaka, S. & Eguchi, T. (1999). Superplume Project: towards a new view of whole Earth dynamics. *Earth, Planets, Space* **51**, i–v.
- Janney, P. E., Le Roex, A. P., Carlson, R. W. & Viljoen, K. S. (2002). A chemical and multi-isotope study of the Western Cape melilitite province, South Africa: implications for the sources of kimberlites and the origin of the HIMU signature in Africa. *Journal of Petrology* **43**, 2339–2370.
- Kalt, A., Hegner, E. & Satir, M. (1997). Nd, Sr, and Pb isotopic evidence for diverse lithospheric mantle sources of East African Rift carbonatites. *Tectonophysics* **278**, 31–45.
- Karson, J. A. & Curtis, P. C. (1994). Quaternary volcanic centers of the Turkana Rift, Kenya. *Journal of African Earth Science* **18**, 15–35.
- Kieffer, B., Arndt, N., LaPierre, H., Bastien, F., Bosch, D., Pecher, A., Yirgu, G., Ayalew, D., Weis, D., Jerram, D. A., Keller, F. & Meugniot, C. (2004). Flood and shield basalts from Ethiopia: magmas from the African Superswell. *Journal of Petrology* **45**, 793–834.
- Koppers, A. (2002). ArArCALC—software for $^{40}\text{Ar}/^{39}\text{Ar}$ age calculations. *Computers and Geosciences* **28**, 605–619.
- Kushiro, I. (1996). Partial melting of a fertile mantle peridotite at high pressures: an experimental study using aggregates of diamond. In: Basu, A. & Hart, S. (eds) *Earth Processes: Reading the Isotopic Code. Geophysical Monograph, American Geophysical Union* **95**, 109–122.
- Lassiter, J. C., Blichert-Toft, J., Hauri, E. H. & Barszczus, H. G. (2003). Isotope and trace element variations in lavas from Raivavae and Rapa, Cook–Austral Islands: constraints on the nature of HIMU- and EM-mantle and the origin of mid-plate volcanism in French Polynesia. *Chemical Geology* **202**, 115–138.
- Le Maitre, R. W. (1976). A new approach to the classification of igneous rocks using the basalt–andesite–dacite–rhyolite suite as an example. *Contributions to Mineralogy and Petrology* **56**, 191–203.
- Le Roux, P., le Roex, A. & Schilling, J.-G. (2002). MORB melting processes beneath the southern Mid-Atlantic Ridge (40–55°S): a role for mantle plume-derived pyroxenite. *Contributions to Mineralogy and Petrology* **144**, 206–229.
- Macdonald, R., Rogers, N. W., Fitton, J. G., Black, S. & Smith, M. (2001). Plume–lithosphere interactions in the generation of the basalts of the Kenya Rift, East Africa. *Journal of Petrology* **42**, 877–900.
- Marty, B., Appora, I., Barrat, J.-A., Deniel, C., Vellutini, P., & Vidal, P. (1993). He, Ar, Sr, Nd and Pb isotopes in volcanic rocks from Afar: evidence for a primitive mantle component and constraints on magmatic sources. *Geochemical Journal* **27**, 223–232.
- Marty, B., Pik, R., & Yirgu, G. (1996). Helium isotopic variations in Ethiopian plume lavas: nature of magmatic sources and limit on lower mantle contribution. *Earth and Planetary Science Letters* **144**, 223–237.
- McKenzie, D. P. & Bickle, M. J. (1988). The volume and composition of melt generated by extension of the lithosphere. *Journal of Petrology* **29**, 625–679.
- Min, K., Mundil, R., Renne, P. R. & Ludwig, K. R. (2000). A test for systematic errors in $^{40}\text{Ar}/^{39}\text{Ar}$ geochronology through comparison with U–Pb analysis of a 1:1 Ga rhyolite. *Geochimica et Cosmochimica Acta* **64**, 73–98.
- Montelli, R., Nolet, G., Dahlen, F. A., Masters, G., Engdahl, E. R. & Hung, S.-H. (2004). Finite-frequency tomography reveals a variety of plumes in the mantle. *Science* **303**, 388–343.
- Morley, C. K. (1994). Interaction of deep and shallow processes in the evolution of the Kenya rift. *Tectonophysics* **236**, 81–91.
- Morley, C. K., Wescott, W. A., Stone, D. M., Harper, R. M., Wigger, S. T. & Karanja, F. M. (1992). Tectonic evolution of the northern Kenya Rift. *Journal of the Geological Society, London* **149**, 333–348.
- Ni, S., Tan, E., Gurnis, M. & Helmberger, D. (2002). Sharp sides to the African superplume. *Science* **296**, 1850–1852.
- Nyblade, A. A. & Robinson, S. W. (1994). The African superswell. *Geophysical Research Letters*, **21**, 765–768.
- Nyblade, A. A., Owens, T. J., Gurrrola, H., Ritsema, J. & Langston, C. A. (2000). Seismic evidence for a deep upper mantle thermal anomaly beneath east Africa. *Geology* **28**, 599–602.
- Ochieng', J. O., Wilkinson, A. F., Kagasi, J. & Kimomo, S. (1988). *Geology of the Loiyangalani area. Report 107 (Reconnaissance)*. Republic of Kenya Ministry of Environment and Natural Resources, Mines and Geology Department, 53 pp.
- Pickering-Witter, J. & Johnston, A. D. (2000). The effects of variable bulk composition on the melting systematics of fertile peridotitic assemblages. *Contributions to Mineralogy and Petrology* **140**, 190–211.
- Pik, R., Deniel, C., Coulon, C., Yirgu, G. & Marty, B. (1999). Isotopic and trace element signatures of Ethiopian flood basalts; evidence for plume–lithosphere interactions. *Geochimica et Cosmochimica Acta* **63**, 2263–2279.
- Renne, P. R., Swisher, C. C., Deine, A. L., Karner, D. B., Owens, T. L. & DePaolo, D. J. (1998). Intercalibration of standard, absolute ages and uncertainties in $^{40}\text{Ar}/^{39}\text{Ar}$ dating. *Chemical Geology* **145**, 117–152.
- Ritsema, J., van Heijst, H. J., & Woodhouse, J. H. (1999). Complex shear wave velocity structure imaged beneath Africa and Iceland. *Science* **286**, 1925–1928.
- Rogers, N., Macdonald, R., Fitton, J. G., George, R., Smith, M. & Barreiro, B. (2000). Two mantle plumes beneath the East African rift system: Sr, Nd and Pb isotope evidence from Kenya Rift basalts. *Earth and Planetary Science Letters* **176**, 387–400.
- Rudnick, R. L., McDonough, W. F. & Chappell, B. W. (1993). Carbonatite metasomatism in the northern Tanzanian mantle: petrographic and geochemical characteristics. *Earth and Planetary Science Letters* **114**, 463–475.
- Samuel, H. & Farnetani, C. G. (2003). Thermochemical convection and helium concentrations in mantle plumes. *Earth and Planetary Science Letters* **207**, 39–56.
- Scarsi, P. & Craig, H. (1996). Helium isotope ratios in Ethiopian Rift basalts. *Earth and Planetary Science Letters* **144**, 505–516.
- Schilling, J.-G., Kingsley, R. H., Hanan, B. B. & McCully, B. L. (1998). Nd–Sr–Pb isotopic variations along the Gulf of Aden: evidence for Afar mantle plume–continental lithosphere interaction. *Journal of Geophysical Research* **97**, 10927–10966.
- Shaw, J. E., Baker, J. A., Menzies, M. A., Thirlwall, M. F. & Ibrahim, K. M. (2003). Petrogenesis of the largest intraplate volcanic field on the Arabian Plate (Jordan): a mixed lithosphere–asthenosphere source activated by lithospheric extension. *Journal of Petrology* **44**, 1657–1679.
- Simiyu, S. M. & Keller, G. R. (1997). An integrated analysis of lithospheric structure across the East African plateau based on gravity anomalies and recent seismic studies. *Tectonophysics* **278**, 291–313.
- Simonetti, A. & Bell, K. (1995). Nd, Pb and Sr isotopic data from the Mount Elgon volcano, eastern Uganda–western Kenya: implications for the origin and evolution of nephelinite lavas. *Lithos* **36**, 141–153.

- Sobolev, A. V., Hofmann, A. W., Sobolev, S. V. & Nikogosian, I. K. (2005). An olivine-free mantle source of Hawaiian shield basalts. *Nature* **434**, 590–597.
- Späth, A., Le Roex, A. P. & Opiyo-Akech, N. (2001). Plume–lithosphere interaction and the origin of continental rift-related alkali volcanism—the Chyulu Hills volcanic province, southern Kenya. *Journal of Petrology* **42**, 765–787.
- Steiger, R. H. & Jager, E. (1977). IUGS Subcommission on Geochronology: convention on the use of decay constants in geo- and cosmochronology. *Earth and Planetary Science Letters* **36**, 359–62.
- Stewart, K. & Rogers, N. (1996). Mantle plume and lithosphere contributions to basalts from southern Ethiopia. *Earth and Planetary Science Letters* **139**, 195–211.
- Stracke, A., Hofmann, A. W. & Hart, S. R. (2005). FOZO, HIMU, and the rest of the mantle zoo. *Geochemistry, Geophysics, Geosystems* **6**, Q05007, doi:10.1029/2004GC000824.
- Sun, S.-S. & McDonough, W. F. (1989). Chemical and isotopic systematics of oceanic basalts: implications for mantle composition and processes. In: Saunders, A. D. & Norry, M. J. (eds) *Magmatism in the Ocean Basins*. Geological Society, London, *Special Publications* **42**, 313–345.
- Thiessen, R., Burke, K. & Kidd, W. S. F. (1979). African hotspots and their relation to the underlying mantle. *Geology* **7**, 263–266.
- Thirlwall, M. F. (2002). Multicollector ICP-MS analysis of Pb isotopes using a ^{207}Pb – ^{204}Pb double spike demonstrates up to 4000 ppm/amu systematic errors in Tl-normalization. *Chemical Geology* **184**, 255–279.
- Thompson, R. N. & Gibson, S. A. (2000). Transient high temperatures in mantle plume heads inferred from magnesium olivines in Phanerozoic picrites. *Nature* **407**, 502–506.
- Todt, W., Cliff, R. A., Hanser, A. & Hofmann, A. W. (1996). Evaluation of a ^{202}Pb – ^{203}Pb double spike for high precision lead isotope analysis. In: Basu, A. & Hart, S. (eds) *Earth Processes: Reading the Isotopic Code*. *Geophysical Monograph, American Geophysical Union* **95**, 429–437.
- Trua, T., Deniel, C. & Mazzuoli, R. (1999). Crustal control in the genesis of Plio-Quaternary bimodal magmatism of the Main Ethiopian Rift (MER): geochemical and isotopic (Sr, Nd, Pb) evidence. *Chemical Geology* **155**, 201–231.
- Volker, F., Altherr, R., Jochum, K.-P. & McCulloch, M. T. (1997). Quaternary volcanic activity of the southern Red Sea: new data and assessment of models on magma sources and Afar plume–lithosphere interaction. *Tectonophysics* **278**, 15–29.
- Walsh, J. & Dodson, R. G. (1969). *Geology of Northern Turkana*. Report of the Geological Survey of Kenya **82**, 42 pp.
- Weeraratne, D. S., Forsyth, D. W., Fisher, K. M. & Nyblade, A. A. (2003). Evidence for an upper mantle plume beneath the Tanzanian Craton from Rayleigh wave tomography. *Journal of Geophysical Research* **108**, doi: 10.1029/2002JB002273.
- White, W. M., Albarède, F. & Télouk, P. (2000). High-precision analysis of Pb isotopic ratios using multi-collector ICP-MS. *Chemical Geology* **167**, 257–270.
- Wilkinson, A. F. (1988). Geology of the Allia Bay area. Report 109 (*Reconnaissance*). Republic of Kenya Ministry of Environment and Natural Resources, Mines and Geology Department, 54 pp.
- Yaxley, E. M., Crawford, A. J. & Green, D. H. (1991). Evidence for carbonatite metasomatism in spinel peridotite xenoliths from western Victoria, Australia. *Earth and Planetary Science Letters* **107**, 305–317.
- Zack, T., Foley, S. F. & Jenner, G. A. (1997). A consistent partition coefficient set for clinopyroxene, amphibole and garnet from laser ablation microprobe analysis of garnet pyroxenites from Kakanui, New Zealand. *Neues Jahrbuch für Mineralogie, Abhandlungen* **172**, 23–41.
- Zanettin, B., Justin Visentin, E., Bellieni, G., Piccirillo, E. M. & Francesca, R. (1983). The volcanism of the North Turkana Basin, Kenya; age, succession and structural evolution. *Bulletin des Centres de Recherches Exploration–Production Elf-Aquitaine* **7**, 249–255.
- Zhao, D. (2001). Seismic structure and origin of hotspots and mantle plumes. *Earth and Planetary Science Letters* **192**, 251–265.

APPENDIX: ANALYTICAL METHODS

Bulk-rock analyses for major and minor elements (including Ba and Sr) were obtained by DCP on an ARL-Fisons Spectraspan 7; P_2O_5 and remaining trace elements were analyzed by ICP-MS using a VG PlasmaQuad-3 at Duke University. Precision based on replicate analyses of samples and natural basalt standards is generally <1% for SiO_2 , Sr, Y, Zr, Nb, La and Ce; <3% for other major elements, Ba, Sr, Rb, Cs, Cr, Sc, V, Co, Pr, Nd, Sm, Eu, Gd, Tb, Dy, Ho, Er, Hf and Ta; <5% Ni, Yb, Lu, Pb and Th; and <8% for U.

Strontium isotopic compositions are corrected with an internal normalization of $^{86}\text{Sr}/^{88}\text{Sr} = 0.1194$. Nd isotopic compositions were normalized to $^{146}\text{Nd}/^{144}\text{Nd} = 0.7219$ to correct for within-run fractionation; ϵ_{Nd} values are reported in this study relative to the chondritic uniform reservoir (CHUR) value of 0.512638. Sr and Nd isotopic standards were routinely run to monitor analytical performance. Average NIST SRM 987 was $^{87}\text{Sr}/^{86}\text{Sr} = 0.710240$ (0.000012, 2σ , $n = 2$); average La Jolla was $^{143}\text{Nd}/^{144}\text{Nd} = 0.511850$ (0.000020, 2σ , $n = 4$). NIST SRM 981 was analyzed at UCLA to monitor machine performance and to provide a means for fractionation correction. Average NIST SRM 981 values were $^{206}\text{Pb}/^{204}\text{Pb} = 16.896$ (0.007, 2σ , $n = 3$), $^{207}\text{Pb}/^{204}\text{Pb} = 15.435$ (0.004, 2σ , $n = 3$), and $^{208}\text{Pb}/^{204}\text{Pb} = 36.5333$ (0.010, 2σ , $n = 3$).

The Pb isotope compositions analyzed at SDSU were determined by MC-ICP-MS on the Nu Plasma HR using the Tl doping technique using NIST SRM 997 Tl (White *et al.*, 2000; Albarède *et al.*, 2004) and $^{205}\text{Tl}/^{203}\text{Tl} = 2.3889$ (Thirlwall, 2002) to monitor fractionation. The Tl-corrected NIST SRM 981 Pb standard averaged $^{206}\text{Pb}/^{204}\text{Pb} = 16.9267 \pm 0.0002$, $^{207}\text{Pb}/^{204}\text{Pb} = 15.4781 \pm 0.0002$, and $^{208}\text{Pb}/^{204}\text{Pb} = 36.6553 \pm 0.0008$ during the analysis period. The NIST 981 standard was run every third analysis. The sample Pb isotope ratios were corrected for instrumental mass fractionation and machine bias using the bracketing standard runs and a delta correction to the Todt *et al.* (1996) values for NIST 981. Uncertainties reported on the measured isotope ratios represent error propagation of the in-run $2\sigma/\sqrt{n}$ analytical errors plus the $2\sigma/\sqrt{n}$ reproducibility of the standard.

Argon–argon dates shown are weighted mean plateau ages determined on fine-grained whole-rock samples. Samples were leached to remove minor alteration

products by washing in 5% HF for 30 s, followed by a water rinse, ultrasound in dilute nitric acid for 20 min, another water rinse, and then drying. Cleaned samples were examined under a binocular microscope and altered crystals removed by hand. All samples were irradiated in quartz vials at the Oregon State University TRIGA research reactor; neutron fluence was monitored with the Fish Canyon Tuff biotite standard (28.03 ± 0.16 Ma, Renne *et al.*, 1998). Typical irradiation conditions were 6 h in a dummy fuel rod in the reactor's central ring, at 1 MW power. Following irradiation and initial decay of short-lived radionuclides, samples were loaded in an ultrahigh-vacuum gas extraction line. After gas clean-up with Zr–Al getters the isotopic composition of Ar released at each heating step was measured with a MAP 215/50 mass spectrometer. Samples were heated in 50–100°C increments, from 400°C to fusion in 6–13 steps, depending on K content. Ar data were acquired in a peak-hopping mode (for $m/z = 35, 36, 37, 38, 39, 40$) by computer. Peak decay was linear and typically <10% over 12 sets of peaks and backgrounds. Mass discrimination on the MAP system was measured with zero age samples run in the same way as samples, and was constant at 1.005 (for 2 a.m.u.). The sensitivity of the mass spectrometer is 4×10^{-14} mol/V and measured backgrounds were 1.5×10^{-18} mol at $m/z = 36,$

2×10^{-18} mol at $m/z = 39$ and 1.5×10^{-16} mol at $m/z = 40$. Procedure blanks for the resistance furnace ranged from 3.0×10^{-18} mol ^{36}Ar and 9.0×10^{-16} mol ^{40}Ar at 600°C to 6.4×10^{-18} mol ^{36}Ar and 1.9×10^{-15} mol ^{40}Ar at 1400°C, whereas laser chamber blanks measured before each sample and after every third step during sample analysis were $(2\text{--}3) \times 10^{-18}$ mol ^{36}Ar and $(6\text{--}9) \times 10^{-16}$ mol ^{40}Ar . ArArCALC v2.2 software from Koppers (2002) was used to reduce data and make plots. Step ages were calculated using the corrected Steiger & Jäger (1977) decay constant of $5.530 \pm 0.097 \times 10^{-10}$ yr $^{-1}$ (2σ) as reported by Min *et al.* (2000), assuming that initial sample Ar compositions were atmospheric (initial $^{40}\text{Ar}/^{36}\text{Ar} = 295.5$), and plotted against cumulative proportion of gas released (per cent ^{39}Ar) as age spectrum, or 'plateau' diagrams.

For He isotope analysis, olivine phenocrysts were obtained from lightly crushed rocks by sieving and hand-picking under a binocular microscope. Grains were cleaned ultrasonically in deionized water and then in acetone, then air-dried and re-examined under the microscope. Crystals showing evidence of alteration or adhering rock matrix were rejected. Olivine separates were analyzed by *in vacuo* crushing to liberate gases trapped within melt and/or fluid inclusions as described by Graham *et al.* (1998).